

Nanoelectronics Lithography

Stephen Knight
National Institute of
Standards and Technology

Vivek Prabhu
National Institute of
Standards and Technology

John H. Burnett
National Institute of
Standards and Technology

James Alexander Liddle
National Institute of
Standards and Technology

Christopher Soles
National Institute of
Standards and Technology

Alain C. Diebold
University at Albany

19.1	Introduction	19-1
19.2	Photoresist Technology.....	19-3
	Fundamentals • Advances by Material Structure • Progress in Resists for EUV • Progress in Resists for 193 nm Immersion Lithography • Concluding Remarks	
19.3	Deep Ultraviolet Lithography.....	19-8
	DUV Lithography Steppers • 193 nm Immersion Lithography • Double Patterning • Ultimate Resolution Limits of DUV Lithography	
19.4	Electron-Beam Lithography.....	19-14
	Resolution • Throughput • Overlay • Cost of Ownership	
19.5	Nanoimprint Lithography.....	19-17
	Variations of NIL • Fundamental Issues • Overlay Accuracy and Control • Technology Examples • Future Perspectives	
19.6	Metrology for Nanolithography.....	19-24
	Advanced Lithographic Processes • Metrology for Advanced Lithography Processes • Proposed New CD Metrology Methods	
	Abbreviations.....	19-28
	References.....	19-28

Official contribution of the National Institute of Standards and Technology; not subject to copyright in the United States.

Certain commercial equipment and materials are identified in this paper in order to specify adequately the experimental procedure. In no case does such identification imply recommendations by the National Institute of Standards and Technology nor does it imply that the material or equipment identified is necessarily the best available for this purpose.

19.1 Introduction

The modern integrated circuit (IC), comprising memory, logic processors and analog devices are multicomponent and multi-level nanostructures prepared by a series of patterning and pattern-transfer steps. Figure 19.1 shows the cross-sectional hierarchical structure that starts from the smallest feature, the transistor, to dielectrics and metal contacts, that are each well defined and must precisely overlay the previous layer. This three-dimensional nanoelectronics structure is manufactured by a rapid patterning process called lithography.

Since the invention of the transistor in 1947 by Bell Labs and Intel's first microprocessor in 1971, modern lithography has enabled the semiconductor industry to shrink device dimensions. The early progress was first quantified by Gordon Moore

in 1965 and is now known as Moore's law.¹ While progress in all process steps are required to achieve the continual shrinking of circuit elements, the advancements in lithography have been the overwhelming driving force. Figure 19.2 shows how Moore's law has guided the industry's systematic increase in the number of transistors per chip since the introduction of the IC. Indeed, now and in the future, the industry will achieve productivity improvements primarily by feature reduction.²

While a wide variety of lithography technologies have been developed, optical step and repeat lithography technologies are the predominant methods of printing features on the semiconductor surfaces and overlying the interconnect structures. A number of competing technologies have been explored, such as x-ray^{3,4} and flood electron beam (SCALPEL),^{5,6} but optical lithography has dominated through vigorous optical technology and tool developments that have left it the lowest cost solution with highest throughput. Direct-write electron-beam technology provides the highest resolution and remains the leading technique for manufacturing the masks used by optical lithography. A novel way of comparing different lithography strategies is by a plot of resolution versus throughput, also known as "Tennant's Law,"^{7,8} as plotted in Figure 19.3. In this plot, direct-write approaches, such as single-atom placement by scanning tunneling microscopy (STM), atomic-force

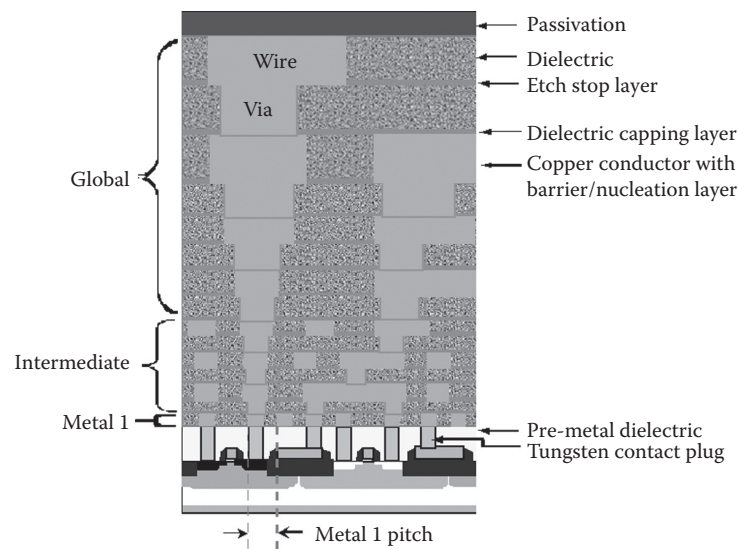


FIGURE 19.1 Cross section of an integrated circuit, showing the active semiconductor and multilayer interconnect levels. (Reproduced from *International Technology Roadmap for Semiconductors*, 2007 edition, SEMATECH, Austin, TX, Figure INTC2, 2007. With permission.)

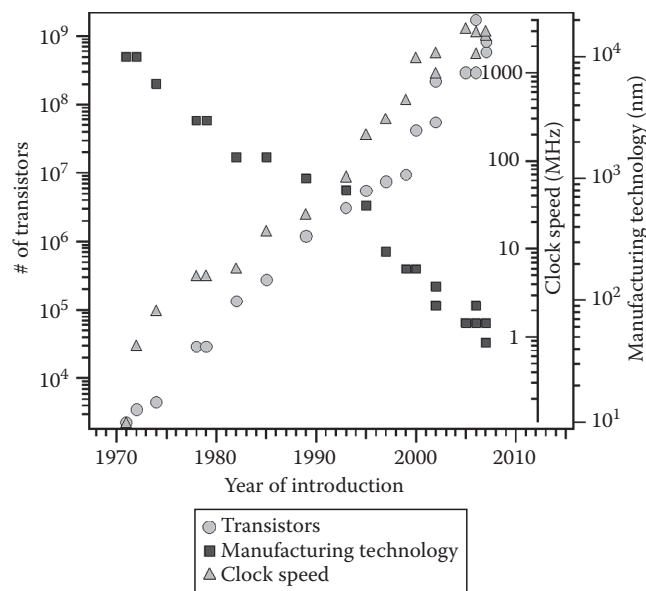


FIGURE 19.2 A composite plot of the scaling of the number of transistors, clock speed, and manufacturing technology versus the year of introduction of Intel Processors. (Data from www.intel.com/technology/timeline.pdf. With permission.)

microscopy (AFM) tip-induced oxidation, and electron-beam lithography are compared with optical steps and repeat lithography that replicate the features of a mask. The continued advancements in optical lithography have pushed the resolution to smaller features at higher pixel throughput, as analyzed by Brunner.⁹

The fundamental guide for optical step and repeat lithography is the Rayleigh equation, which provides the scaling criteria for predicting the smallest optically definable image²

$$R = k_1 \frac{\lambda}{NA} = k_1 \frac{\lambda}{n \sin \theta}; \quad (19.1)$$

where

λ is the source wavelength

n is the medium refractive index

$n \sin \theta$ is the numerical aperture (NA) with the incidence angle (θ)

k_1 is a process dependent factor

While the Rayleigh equation defines the resolution, the ability of the photoresist to replicate the mask features is of critical importance. All approaches and manufacturing tools have taken advantage of the Rayleigh equation to predict transitions from each manufacturing technology node (smallest feature size) up to the diffraction limit. Optical lithography started with the near *ultraviolet* (UV) g-line (436 nm) and i-lines (365 nm) of mercury-arc lamps and made way for laser sources in the deep *ultraviolet* (DUV) from KrF (248 nm) and ArF (193 nm) excimers. A significant extension, immersion lithography, decreases the 193 nm wavelength by using water as the immersion fluid and is on track to produce features down to 32 nm. The next-generation photoresist materials, described in Section 19.2, for sub 22 nm features expect to image 13.4 nm radiation in extreme *ultraviolet* (EUV) with all reflective lithography imaging tools.

While most of this chapter focuses on the leading-edge and next-generation technologies used for defining the finest features in nanoelectronics, it is important to recognize that for most applications it is necessary to connect the nano-world (transistor) to the macro-world (a computer motherboard). Figure 19.1 shows the cross section of an IC. Note, however, that the interconnect sizes increase at subsequent higher levels. Therefore, the previous-generation tools continue to play crucial roles by migrating to the higher levels of interconnect.

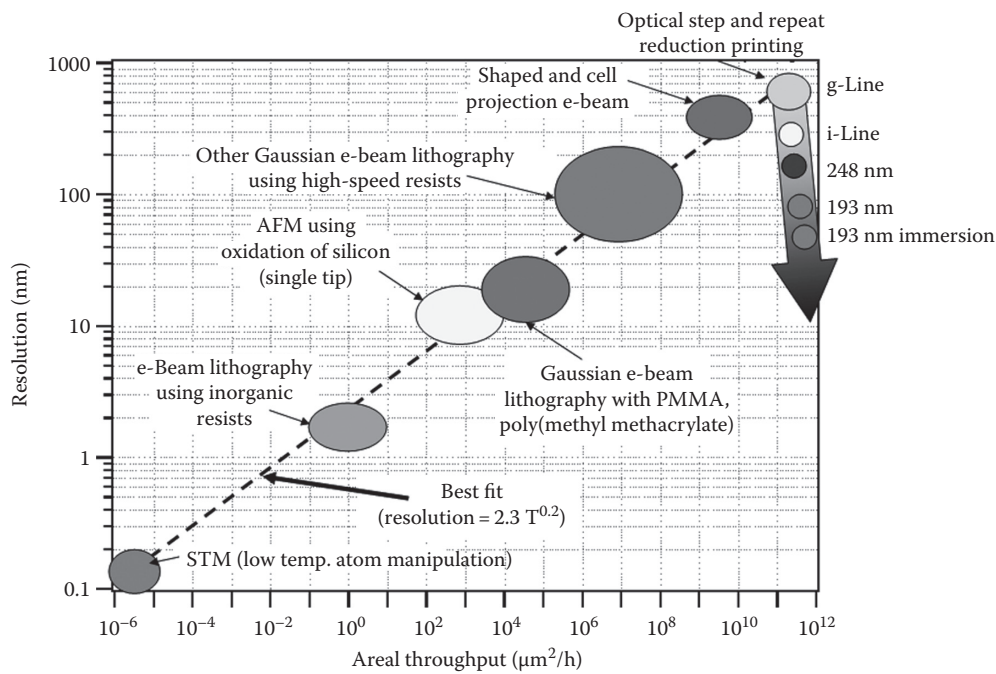


FIGURE 19.3 “Tennant’s Law,” whereby the resolution (R) versus areal throughput (T) scales as $R = 2.3 T^{0.2}$, the progress of optical step and repeat lithography has driven to higher resolution and throughput. (Adapted from Tennant, D., *Limits of conventional lithography*, in Timp, G.M. (ed), *Nanotechnology*, AIP Press, New York, Chapter 4, p. 161, 1999. With permission.)

Microelectronics and now nanoelectronics technology have become a collaborative and competitive worldwide effort, as exemplified by the *International Technology Roadmap for Semiconductors* (ITRS), available to the public at <http://www.itrs.net>. The ITRS is updated every two years by subject matter experts from the semiconductor manufacturing industry, the tool and materials supplier industries, the factory automation infrastructure, academia, and government agencies. An important guiding aspect of the ITRS roadmap is the identification of the status of the technology nodes and guidance of the phases of research, development, and pre-production. In particular, the 2007 edition identifies potential lithographic solutions out to 2022, with a predicted dynamic random access memory half pitch of 11 nm and FLASH memory half pitch of 9 nm as shown in Figure 19.4.

In this roadmap, several emerging lithography approaches are highlighted. Double patterning with 193 nm DUV water immersion is expected to extend to the 32 nm half pitch era with high-volume production in 2013. Alternatively, contending technologies for 22 nm half pitch are EUV Lithography, 193 nm DUV immersion with higher index fluid and lens materials, maskless lithography (ML2), and nanoimprint lithography (NIL).^{10,11} NIL is rapidly emerging as a low-cost, high-resolution, and versatile alternative to optical lithography. Below 22 nm half-pitch, the likely technology solutions are less clear. All the technologies mentioned above, along with new contenders, such as directed self assembly, have credible paths. However, each would have to surmount numerous technical difficulties while limiting exorbitant cost and loss in throughput.

In the rest of this chapter, we describe some of the challenges facing the photoresist materials (Section 19.2) used in optical lithography including some crucial aspects facing these materials as the feature dimensions are reduced to the length scale of the basic photoresist polymers. In Section 19.3, DUV lithography, the basic optics, advancements in steppers, and approaches to extend to higher-resolution, denser features are described. In Section 19.4, electron-beam lithography is covered with respect to the metrics of resolution, throughput, overlay requirements, and cost. Section 19.5 highlights a nonoptical lithography approach, NIL. In this section, several variations of NIL for transferring mask features into a photoresist are described. Finally, in Section 19.6, we end with an overview of the metrology requirements for nanolithography. Figure 19.1 is a reminder that one must print and measure a wide-range of feature dimensions, from the nanoscale to the macroscale. Lastly, a separate chapter in this handbook is dedicated to EUV lithography.

19.2 Photoresist Technology

The optical image projected from a mask upon a thin film at the semiconductor wafer plane is the first step of photolithography.^{10,12} The thin films that replicate the mask features are called photoresists with basic process as shown in Figure 19.5. The high sensitivity of photoresists to radiation have consistently met the challenges of smaller, high-fidelity features with increased throughput driven by memory and processor chip performance to feature size gains (Moore’s law). The etch resistance of the

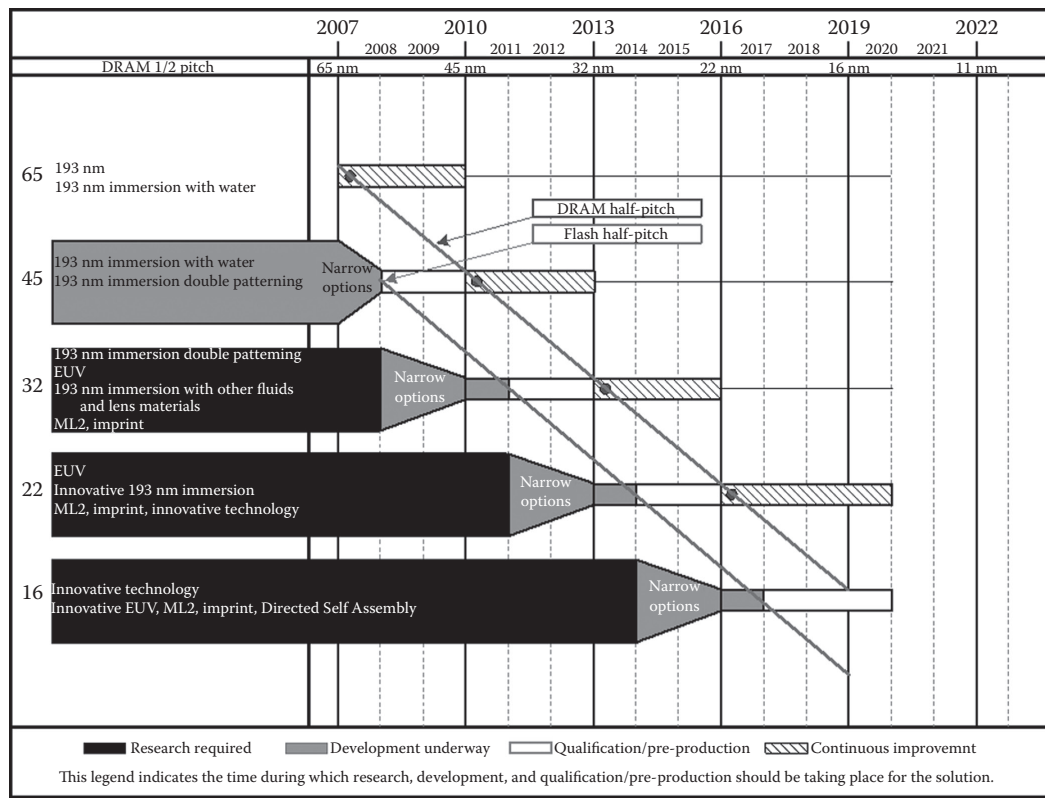


FIGURE 19.4 Roadmap for half pitch scaling. (Reproduced from *International Technology Roadmap for Semiconductors*, 2007 edition, SEMATECH, Austin, TX, Figure LITH5, 2007. With permission.)

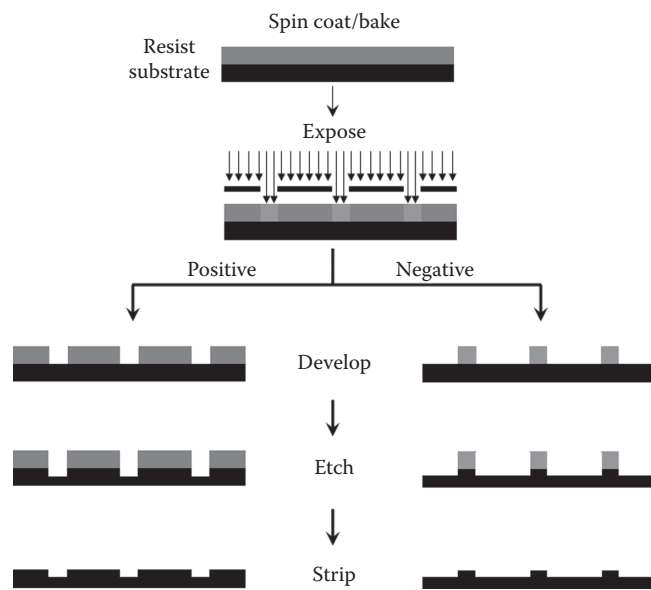


FIGURE 19.5 Schematic of the lithographic process for positive and negative tone resist.

photoresist allows pattern transfer into the underlying semiconductor wafer.

Test structures, such as a line and space pattern as shown in Figure 19.6, must meet criteria as defined by the ITRS roadmap for critical dimension (CD). The CD is the feature

size, for example, in a 32 nm half-pitch 1:1 dense line, a line with a width of 32 nm is followed by a space of equal size. The Rayleigh equation defines the resolution; however, the ability of the photoresist to perfectly replicate the mask features is of critical importance. The line-width variations called line-width roughness (LWR) and line-edge roughness (LER) must be reduced to less than 2 nm for 32 nm half pitch (HP) as they impact device performance.^{13,14} Therefore, the photoresist materials chemistry plays a substantial role for both resolution and LER. Methods to extend resist resolution by double patterning methods and new photoresist architectures must be leveraged against meeting the LER requirements for sub-22 nm lithography.

19.2.1 Fundamentals

The requirements for advanced photoresists are discussed in the 2007 ITRS roadmap.¹⁴ Specifically, the “Lithography” chapter highlights difficult challenges:

- Resist materials at <32 nm indicates three issues (1) Resist and antireflective coating materials composed of alternatives to PFAS [perfluoroalkylsulfonate] compounds, (2) Limits of chemically amplified resist sensitivity for <32 nm half-pitch due to acid diffusion length, and (3) materials with improved dimensional and LWR control.

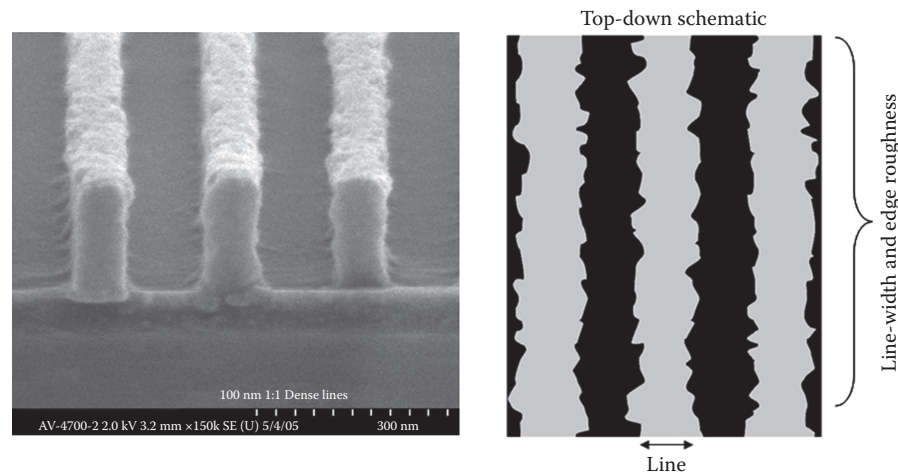


FIGURE 19.6 Example of a cross-sectional SEM image of a 100 nm 1:1 line-space lithographic line. The fluctuations in the feature critical dimension along the line are quantified by line-edge roughness and line-width roughness metrics as indicated in the schematic.

The details of the photoresist materials chemistry are at the heart of turning the optically defined patterns into three-dimensional nanoscale features. Chemically amplified photoresists are formulations of an acid-sensitive polymer film mixed with photoacid generators (PAGs) and other additives, such as base quenchers. Upon exposure through a mask, strong acids are formed by photolysis of the molecularly mixed PAG within the thin film. A post-exposure bake is then applied and the acidic protons (photoacids) diffuse along with the counter-anions and catalyze a deprotection reaction on the acid-sensitive polymer to change the local solubility for development in an aqueous hydroxide solution as shown in Figure 19.7. The photoacids are true catalysts as they are regenerated by each deprotection reaction;¹⁵ hence, the term chemical amplification refers to the cascade of reactions that occur within the photoresist induced by a single photon. Therefore, these photoresists may be used at low exposure doses.

The chemical reaction-diffusion that forms the latent image and development must be understood and controlled at the nanometer length scale. Chemically amplified photoresists are also deposited onto bottom anti-reflection coatings (BARC) to eliminate the effects of standing waves. Interactions and component transport between the BARC and resist layer can lead to loss of profile control or pattern collapse and therefore must also be understood. Detailed studies of these interactions and transport mechanisms are needed to design materials for the successful fabrication of sub-32 nm structures.

As feature sizes are reduced to below 32 nm, a general problem of simultaneously minimizing dose sensitivity, CD, and LER was observed experimentally and theoretically. These observations suggest only two of these metrics may be met at the sacrifice of the third. Several theoretical models¹⁶⁻¹⁸ have been proposed, such as those by Bristol (2007)

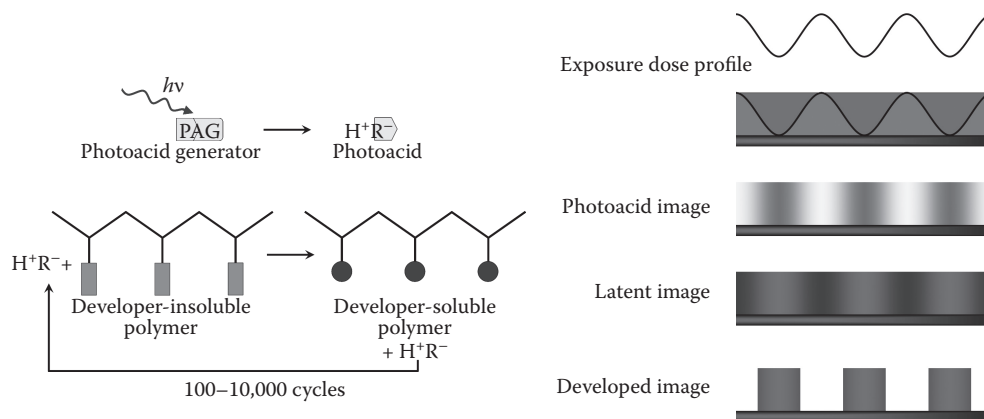


FIGURE 19.7 Schematic of the photolysis process of a photoacid generator that forms a strong acid (H^+R^-) and the subsequent acid catalytic reaction that changes the solubility of the polymer in a developer solution. Schematic of the mask-defined dose profile, subsequent profile in the photoresist film that leads to a photoacid image and chemical latent image formed during the post-exposure bake. The final developed image is formed after selective dissolution in a developer solution as determined by the extent of chemical reaction in the nominally exposed regions.

$$\text{LER} \approx \frac{1}{\sqrt{q\alpha D_e}} \sqrt{1 + \frac{1}{\epsilon} \frac{1}{\text{LILS} \cdot \delta}}, \quad (19.2)$$

where

- q is the number of photons/nm²
- D_e is the dose at the line-edge (threshold for development)
- α is the fraction of light absorbed
- ϵ is the quantum efficiency defined by the (molecules of acids produced)/(number of absorbed photons)
- δ is the effective photoacid diffusion length
- LILS is the latent-image log slope

As shown in the schematic of Figure 19.7, the initial photoacid image is followed by a post-exposure bake step whereby the photoacid diffuses and reacts. The extent of the reaction will define a chemical latent image in the photoresist. The local slope of the chemical transformation, or latent-image log slope (LILS), at the point of development is critical to maximize. Qualitatively, a large exposure dose leads to a lower LER at fixed LILS and δ . However, notice that once smaller features are desired ($\delta < \text{CD}$), then the photoacid diffusion length should be reduced; hence at fixed D_e , a smaller δ may increase LER. The full problem is a nonlinear reaction-diffusion equation and typically requires additional parameterization to include the effects of photoacid loss, photoacid trapping, and amine quenchers that react and diffuse. However, approaches such as Equation 19.2 provide qualitative insights into the resist problem. In cases when the material specifics were not known, the form of material constant = (half-pitch)³ × (LER)² × (Sensitivity) has been used.¹⁹

Such resolution limits are linked to the fundamentals of photoacid generation (via D_e , α , ϵ) and chemical reaction-diffusion during the post-exposure bake that defines the LILS, choice of photoresist chemistry, PAG size, and processing time and the temperature that ultimately determines the photoacid diffusion length and development step that resolves the final feature. Experimental methods have been developed to quantitatively measure many of these parameters. More recently, parameters such as the photoacid diffusion length were estimated by modeling of the lithographic feature power spectrum.¹⁶

The efficient generation of photoacids is also crucial to photoresist technology. Analytical methods have been developed to measure photoacid generation and quantum efficiency.^{20–23} Many of these techniques rely on a well-defined dose upon photoresist thin films followed by analytical approaches to determine the acid concentration via titration with a standard base. More recently, quantifying the quantum efficiency and acid generation mechanisms in EUV photoresists has taken a more important role as increasing the acid concentration or efficiency (Equation 19.2) is a method for reducing LER. For 248 and 193 nm lithography, photoresist polymers were designed for low absorbance, while the PAG absorbs strongly for photolysis. Since organic photoresist polymers absorb strongly in the EUV, the photolysis induced by the direct exposure of

the 92 eV photon and secondary electrons are equally important. In fact, the ϵ for EUV exposure is greater than 1 due to the non-negligible contribution from lower energy secondary electrons. In both DUV and EUV lithography, the photoacid image plays the important role of changing the local solubility of the photoresist polymer in the nominally exposed regions (Figure 19.7).

During the post-exposure bake, the latent image (Figure 19.7) formed is a composition profile of the photoresist within the line:space feature. The true shape of this profile is due to the photoacid catalyzed reaction-diffusion process that cleaves (deprotection) a nonpolar side-group of the photoresist polymer. The influence of the optical image quality on the final developed feature may be probed by varying the aerial image contrast. Hinsberg et al. elegantly showed that the initial photoacid distribution, controlled through the exposure quality by interferometric lithography, significantly affects the printed feature quality.²⁴ Furthermore, using an image-fading technique, Pawloski et al. identified an apparent resolution limit in the final feature of 193 nm resists as quantified by LER versus the image-log slope (ILS).²⁵ These changes in the feature quality are also controlled by the reaction-diffusion of the photoacid¹² into the unexposed regions that leads to image spreading or blurring.²⁶ However, even with an ideal step-exposure condition, mimicked by forming a bilayer stack, the reaction-diffusion process induces an image blur. Controlling the photoacid reaction-diffusion (via LILS and δ) remains an important strategy for improving feature quality.

The transport properties of the photoacid are also influenced by the changes in the local chemical composition that occur during the deprotection reaction.²⁷ Houle et al. demonstrated that the evolving resist polymer chemistry plays a crucial role in lithographic imaging.²⁶ An increased photoacid size decreased the apparent diffusion length,^{28,29} but also quantitatively increased the LILS.^{30,31} However, the catalytic efficiency of the photoacid proton can dominate, such that by increasing the size of the photoacid counter-anion, image blur occurs primarily due to the local proton mobility, not diffusion of the acid-counter-anion pair.³² Neutron reflectivity methods were developed to characterize the shape of the reaction-diffusion front with nanometer resolution.^{14,30,31,33–37} In these studies, the influence of the evolving chemical composition on the spatial-extent of the reaction profile was directly measured.

Base quencher additives are also used in photoresist formulations to limit the reaction and diffusion of the photoacid catalyst into unexposed regions.^{12,38} The influence of these neutralizing species on the reaction-diffusion process is complex.³⁹ The simplistic view of the quenchers solely acting to neutralize photoacid, thus decreasing the acid concentration, is not always correct.⁴⁰ The quencher appears to partially neutralize the photoacid less than stoichiometrically, influence the dissolution either as promoters or inhibitors, and increase the development induction time.³⁹ The partial neutralization initially reduces the amount of acid available after photolysis proportional to the base concentration.^{40–42} The influence

of quenchers on the chemical gradients in the film were suspected to control LER.⁴³ Direct measurements of the effect of amine quenchers on the reaction-diffusion profile shape (LILS) and spatial extent (δ) were determined by neutron reflectivity.³⁵

A central assumption in these resolution limit models is a direct transfer of the chemical deprotection reaction-diffusion heterogeneity on the feature quality; the details of the development process are not considered. However, the bulk of photoresist thin films dissolve via reactive dissolution kinetics involving a well-defined steady-state swollen layer.⁴⁴⁻⁴⁶ This swollen layer must approach the nominally unreacted and unexposed zone as bulk development ceases.⁴⁷ This crucial transition zone results from the initial deprotection latent image that can be controlled by aerial images, polymer chemistry, photoacid generators and base additives, and post-exposure bake conditions.^{30,35} The mechanism of how the advancing swelling dissolution front faces the transition of soluble to insoluble species (solubility switch) is crucial for the understanding of resist resolution limits. This was addressed by neutron reflectivity techniques that directly measured the developer penetration and extent of line-edge swelling.⁴⁸⁻⁵⁰ The residual swelling fraction at the feature edge remains diffuse over length scales (>10 nm) far exceeding the polymer chain dimensions during hydroxide development and water rinse step; the swelling layer eventually collapses upon drying.

Alternative development approaches to control this residual swelling fraction may be needed to smooth and reduce LER.

19.2.2 Advances by Material Structure

In a typical polymer photoresist, the PAG is dissolved along with the photoresist polymer and spin cast to form a thin film mixture, or binary blend. Polymers provide flexible platforms to change functional groups in order to meet etch resistance, optical transparency, refractive index requirements, and a variety of acid-sensitive protecting groups. The high glass transition temperatures (typically, $T_g > 140^\circ\text{C}$) provide dimensional stability and wide latitude in post-exposure bake temperature that increases the rates of reaction and photoacid diffusivity. Lastly, polymers have a large degree of lipophilicity in an aqueous base developer that provides a high-development contrast.¹²

Driven by the CD requirements, it was considered that reducing the photoacid diffusion length would enable smaller CD. The PAG and polymer blend approach may not be the most effective route, since the photoacid could diffuse to lengths longer than the CD. In order to address this viewpoint, an alternative resist structure was devised that covalently bonds the photoacid generator to the polymer as shown in Figure 19.8a.⁵¹⁻⁵⁴ With this approach, after exposure, the photoacid counter-anion remains covalently bound to the polymer thereby restricting the acidic

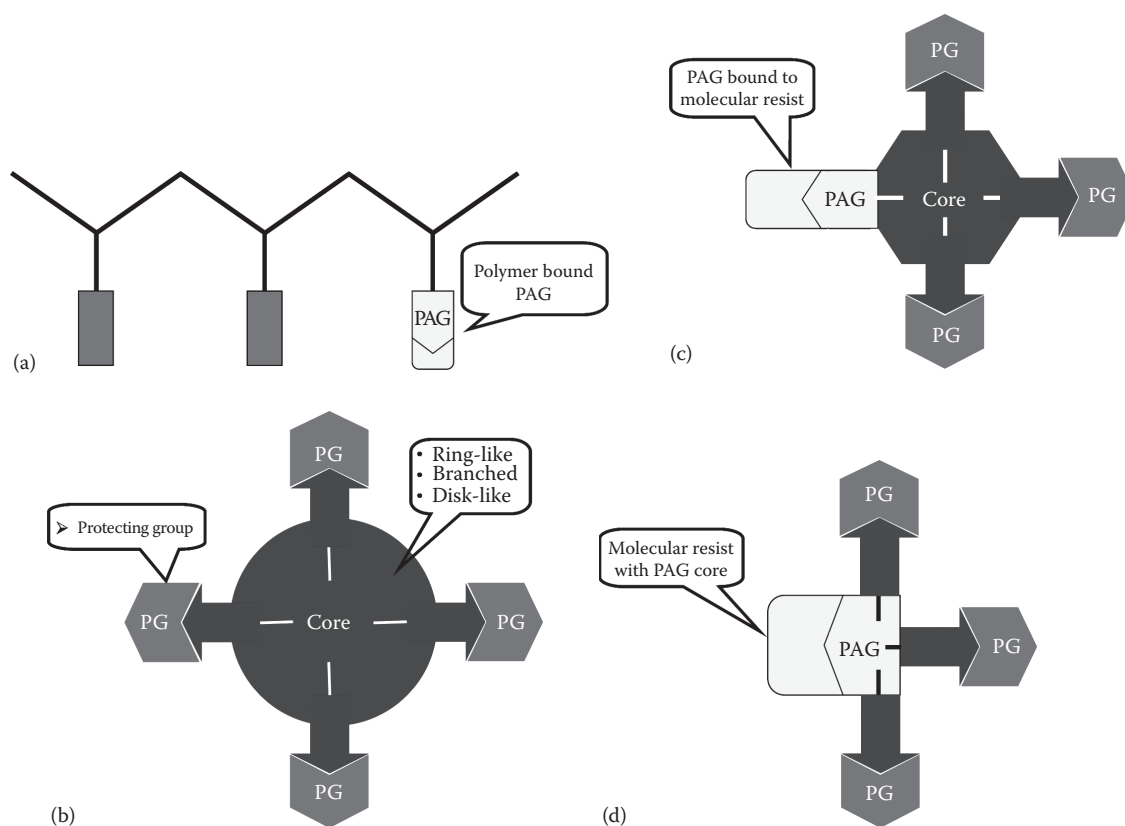


FIGURE 19.8 Cartoons of photoresist architecture alternative to polymer and PAG blends: (a) Photoresist polymer bound to the PAG, (b) molecular glass resist with variable core structure, (c) molecular glass resist bound to the PAG, and (d) PAG-core molecular resist.

proton diffusion length. Such approaches remain promising especially to increase the dose sensitivity.

Since the CD and LER metrics are approaching the characteristic dimensions of the photoresist polymers, alternative architectures were considered to extend photolithography by using lower molar mass molecules.⁵⁵ These molecular glass (MG) resists, while smaller, may also improve the uniformity of blends with PAG and other additives since miscibility of polymer blends decreases with increasing molar mass.⁵⁶ In general, the molecular glass resist has a well-defined small-molecule core that bears protected base-soluble groups (such as hydroxyls and carboxyls) as shown in Figure 19.8b. With this approach, the core chemistry can vary from calix[4]resorcinarenes (ring-like),^{57–59} branched phenolic groups,^{60,61} and hexaphenolic groups (disk-like).^{62,63} Early approaches with MG led to low glass transition temperatures, however, such problems were resolved by increased hydrogen bonding functionality and the design of the core structure. The MG resists may also benefit from a more uniform development due to the lack of chain entanglements and reduced swelling, when compared with polymers; these are active areas of research. Experimental data using the quartz crystal microbalance method demonstrate that swelling appears during development even with molecular glass resists.⁶⁴ Most of these alternative resist structures adhere to the chemical amplification strategy. However, nonchemically amplified photoresists are also being considered as they do not contain photoacid generators and hence do not suffer from photoacid diffusion length constraints.⁶⁵

Two other novel MG variants are a PAG covalently bound to the molecular resist (Figure 19.8c) and the core of the molecule serving as the PAG⁶⁶ (Figure 19.8d). As designed, there would be no need for the blending of PAG with such resist systems. In the case of Figure 19.8d, photolysis produces a photoacid, which then would deprotect the unexposed acid-sensitive protecting groups of the PAG-core molecular glass. These two approaches (Figure 19.8c and d) are smaller pixel sizes and true one-component systems that in principle eliminate surface segregation and phase separation in cast films. These alternate resist structures, however, typically require additives such as amine base quenchers to limit the diffusion of the photoacid catalyst into unexposed regions.

19.2.3 Progress in Resists for EUV

There has been progress in designing photoresists for EUV lithography in anticipation of the 22 nm nodes. The testing and development of new materials typically relies on direct lithographic testing to screen formulations. However, due to the lack of widely available EUV exposure tools, micro-field exposure tools (MET), such as the 0.3 NA SEMATECH Berkeley MET have an important role for resist testing. Substantial progress⁶⁷ in reaching CD challenges with commercial chemically amplified photoresist were reported with 20 nm half-pitch with an EUV dose sensitivity of (12.7–15.2) mJ/cm², which is near the theoretical Rayleigh resolution limit of the 0.3-NA system with

a k_1 of 0.45. While progress in resolution and sensitivity were observed, LER remains a challenge. In fact, the fidelity of the resist feature may have non-negligible LER contributions from the EUV mask and optical trains as ascertained by modeling. After subtracting an estimated mask contribution, resist LER values appear to approach the 2 nm level. Additionally, a pattern collapse of sub-20 nm dense features suggests the intrinsic resolution could be better than expected. In fact, unoptimized model EUV polymers and MG photoresists clearly show 20 nm features as quantified by the latent image and developed image roughness.⁶⁸ Alternative development approaches⁶⁹ may provide new directions to break the resolution limits (Equation 19.2), which currently do not directly consider development effects, such as swelling and swelling layer collapse.

19.2.4 Progress in Resists for 193 nm Immersion Lithography

By inspection, the Rayleigh equation (Equation 19.1) directs that the smallest feature may be achieved by employing higher refractive index media (photoresist and immersion fluids). Currently, highly purified water with $n = 1.44$ is used as the immersion fluid and typical 193 nm polymers have $n \approx 1.7$. The development of photoresists and immersion fluids with higher n are needed. A strategy to increase the refractive index is by incorporating more polarizable heteroatoms, such as sulfur,^{70–73} into the polymer structure. Halides such as Cl, Br, and I would increase the refractive index at the expense of absorption and possible photo-induced side reactions. Developer-soluble top-coat barriers^{74–77} or engineered surface-segregating barrier-layer additives^{78–83} are typically used to reduce or mitigate the leaching of critical components (PAG and quenchers) into the immersion fluid.

19.2.5 Concluding Remarks

Sub-32 nm critical dimensions come with many resist challenges. The challenges of reducing feature size and decreasing LER and sensitivity are inter-related. Current attempts to surpass resolution challenges include novel resist process strategies such as double patterning and double exposure as well as novel architectures. However, it is clear that the quality of the final patterned structures is inter-dependent upon the spatial distribution of the photoacid (optical image quality), the spatial extent of the reaction-diffusion process (latent image), and the development mechanisms. The guidance of the resist resolution metrics in cooperation with improved materials fundamentals will help photoresist materials achieve ever smaller features as suggested by the Rayleigh equation.

19.3 Deep Ultraviolet Lithography

Deep ultraviolet (DUV) lithography, using KrF or ArF excimer lasers with illumination wavelengths of 248 or 193 nm, respectively, is now the predominant technology for producing critical

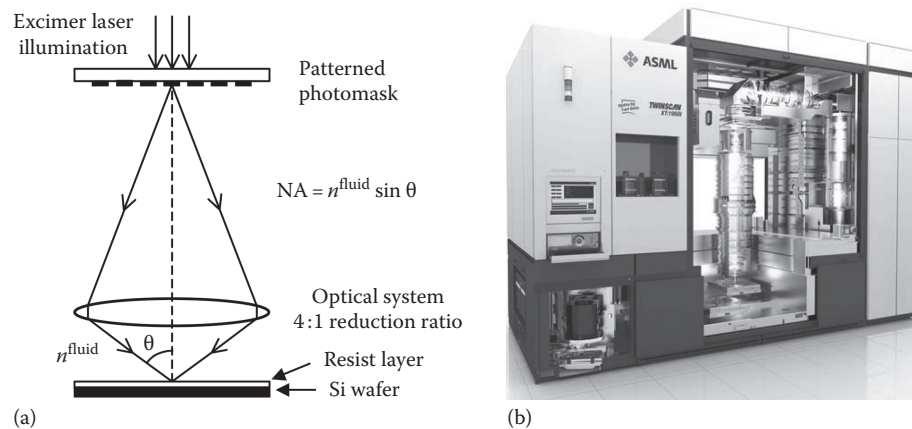


FIGURE 19.9 (a) Schematic of the DUV photolithography exposure process. The numerical aperture is defined by $NA = n^{\text{fluid}} \sin \theta$, where θ is the half angle of the marginal rays and n^{fluid} is the index of the fluid (gas or liquid) between the final lens element and the resist. (b) Illustration of a commercial 193 nm immersion lithography system (ASML TWINSKAN XT:1950i), showing the cylindrical optics barrel in the center, the mask above the optics system, and an illuminated wafer below. (Courtesy of ASML, Veldhoven, Veldhoven, the Netherlands.)

layers of leading-edge, mass-market semiconductor logic and memory ICs. The technology is based on illuminating a patterned fused silica mask with diffused excimer laser radiation and imaging the transmitted light patterns with 4:1 image reduction onto a photosensitive-resist-coated Si wafer, using a diffraction-limited optical system. The process is indicated schematically in Figure 19.9a. The illuminated wafer is removed from the optical system for chemical processing steps to convert the exposed pattern (latent image) in the resist to a patterned structure on the wafer and put back into the optical system multiple times for further exposure/processing steps. State-of-the-art ICs are built up from about 20–30 layers, a significant fraction of which involve DUV exposure steps. An illustration of a leading-edge 193 nm immersion lithography exposure tool for volume production is shown in Figure 19.9b.

DUV lithography is an evolution of optical-projection lithography developed in the late 1960s and the 1970s using the strong spectral lines from mercury discharge lamps to illuminate first at 436 nm (g-line) and later at 365 nm (i-line). In these early systems, the pattern on the mask for the entire circuit was illuminated and imaged onto the wafer for a specified exposure time, and then the wafer was “stepped” to an adjacent unexposed position for another imaging of the circuit pattern. This was repeated until the wafer was filled with as many identical exposures as the wafer size allowed. These wafer “step-and-repeat” systems were termed “steppers.”

In modern leading-edge DUV lithography systems, the full circuit illumination of the mask is replaced by a “scanned” illumination. A fraction of the circuit pattern on the mask is illuminated in a narrow strip across its width and the mask is scanned under this strip, while its image is projected with a 4:1 reduction ratio onto a wafer scanning in the opposite direction, at a speed relative to the mask reduced by the factor of 4. When the full circuit pattern has been exposed, the wafer is stepped to the next position and the process repeated. The exposure image is

stepped-and-scanned across the wafer, producing typically over 50 full chip exposures on a 300 mm diameter wafer at a rate giving about 100 wafers per hour. These wafer “step-and-scan” systems are referred to as “scanners,” though they are often referred to as “steppers” as well.

The first commercially available production optical-projection lithography system, the DSW4800, was introduced by GCA in 1978. It achieved a minimum feature resolution of a little over $1\ \mu\text{m}$ and a slightly larger depth of focus.¹⁰ At the time, it was fully understood that the resolution of the optical-projection lithography approach was fundamentally restricted by the diffraction limit given roughly by the Rayleigh resolution criterion in Equation 19.1. In DUV lithography, the process-dependent factor k_1 is of order 1 Ref. [10,84]. Actually, Equation 19.1 is intended to capture both the limiting effects of diffraction and the impact of the resist processing. Considering just the diffraction effects, Equation 19.1 would refer to the aerial image at the image plane, and k_1 would be determined only by the profile of the light intensity. However, the actual size of a feature ultimately created by the lithography process also depends on the chemical processing of the exposed resist as described in Section 19.2. For an isolated feature, this size can be any value, i.e., k_1 has no fundamental restrictions. On the other hand, for the dense structures of real circuits, e.g., modeled by a periodic structure, the separation between printed features (the pitch) is fundamentally limited. With the minimum feature size in Equation 19.1 defined as half the pitch for a single exposure, k_1 can be rigorously shown to have a minimum value of $k_1 = 0.25$ Ref. [10,84]. This limit holds for any single-exposure process, as long as the process has a linear dose response.

Because a functional circuit must have some topology and because imaging control is imperfect, the resist exposure process requires some finite depth of focus (DOF). This also has a diffraction and geometric limitation, which is characterized by Equation 19.3

$$\begin{aligned} \text{Depth of focus} &= \frac{\lambda}{2n \left(1 - \sqrt{1 - \frac{\text{NA}^2}{n^2}} \right)} \xrightarrow{\text{Small NA}} k_2 \frac{n\lambda}{\text{NA}^2} \\ &= k_2 \frac{\lambda}{n \sin^2 \theta}, \end{aligned} \quad (19.3)$$

where, for small NAs, a process-dependent prefactor k_2 is conventionally used.^{10,84} For large NAs, the exact form of the equation conventionally incorporates a different process-dependent prefactor $k_3 \times 4$.⁸⁵

In the early 1980s, reasonable considerations about the prospect of significantly altering the parameters in Equations 19.1 and 19.3 to improve the resolution and DOF led to the conclusion that optical-projection lithography had an ultimate dense feature size resolution of about $0.5 \mu\text{m}$. Consequently, it was assumed then that progress in high-volume-production ICs would require switching within a decade or so to alternative lithography techniques with more extendibility potential. These included electron-beam direct-write lithography (with multiple parallel beams), electron-projection lithography, ion-projection lithography, x-ray-proximity lithography, extreme-ultraviolet lithography, and nanoimprint lithography.¹⁰ Few people, if anyone, publicly predicted then that the factors in Equations 19.1 and 19.3 would be relentlessly driven to enable optical-projection lithography to out-complete all the alternative technologies mentioned above, in cost and performance capabilities for volume production, at least into the second decade of this century.

19.3.1 DUV Lithography Steppers

A primary driver for this progress has been the wavelength factor in Equation 19.1. This can be seen in Figure 19.10, which shows a log-linear plot of critical feature sizes of leading-edge ICs as a function of year introduced into large-scale production, along with the illumination wavelength used. Wavelength reduction has been aggressively pursued in part because, as is clear from Equations 19.1 and 19.3, feature size reduction by decreasing wavelength reduces DOF less than that by increasing the NA. However, the switch from Hg-arc lamp illuminators with wavelengths at 436 and 365 nm to the DUV excimer laser sources with wavelengths at 248 nm (KrF) around 1995 and 193 nm (ArF) around 2000 was a very challenging one. Hg-arc lamp sources are compact, relatively inexpensive, reliable, and operate continuously. KrF and ArF excimer lasers are much more complex, substantially more expensive to purchase, operate reliably, have undesirable laser coherence properties, and the illumination is pulsed. This last characteristic has been particularly troublesome because obtaining the required exposure doses fast enough for acceptable wafer throughputs requires very high pulse peak intensities. This puts very stringent requirements on the durability of lens and window materials in the optical system. Further, the shorter UV wavelengths substantially limit material

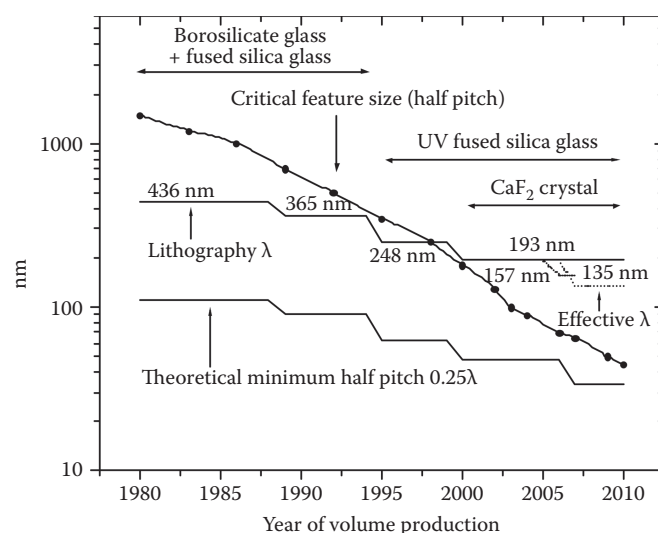


FIGURE 19.10 Plot of critical feature size (half pitch) of leading-edge semiconductor integrated circuits versus year of volume production, on a log-linear plot. Also included is the lithography wavelength used and the theoretical minimum half pitch for single exposures (0.25λ) for this wavelength. 157 nm technology has not been brought into production. Effective λ is λ/n for 193 nm immersion lithography. Optical materials used for lenses at each λ are also indicated.

options for these optical elements. In particular, at the time of the introduction of 248 nm lithography, UV-fused silica glass was the only UV-transmitting material that could meet the tight optical properties specifications for the large lenses required. For 193 nm systems, in addition to UV-fused silica, a second high-quality material, crystalline calcium fluoride (CaF_2), had to be developed for lenses to correct for chromatic aberrations in the optical system due to the wavelength dispersion of the index of fused silica (see Figure 19.10).

Fused silica glass is an amorphous form of SiO_2 , which minimizes the large birefringence effects of the uniaxial crystal structure of crystalline SiO_2 (quartz). However, the amorphous structure makes fused silica a thermodynamically metastable material and it suffers structural changes under exposure to high 193 nm laser intensities. These changes result in both volume compaction and rarefaction effects with different intensity dependencies.⁸⁶ The resulting refractive index and lens geometry changes can substantially degrade lens performance. To minimize these effects, maximum intensities have to be limited throughout the stepper optics, and the more durable CaF_2 lens elements generally must be used in the positions with highest intensities, for example, at the final lens position.

For wavelengths much below 193 nm, UV-fused silica glass has poor transmission, leaving only the cubic structure Group II fluorides as practical lens materials. Of these, only CaF_2 has been made with lithography-grade optical quality. Hence, wavelength extension to 157 nm with F_2 excimer lasers would require the lenses to be made only from CaF_2 , or possibly from other related fluorides, such as BaF_2 , if the optical quality could be

significantly improved.⁸⁷ The availability of lithography-quality CaF_2 for lens material has been a key issue for the development of both 193 and 157 nm lithography technologies, and building a CaF_2 manufacturing infrastructure to support the needs of both of these technologies has been a major challenge. A principal difficulty with CaF_2 production is that its relatively low thermal conductivity and high thermal expansion coefficient requires it to be cooled very slowly from the melt in order to obtain low-strain, single-crystal material of the sufficiently large sizes needed for lenses. Even many weeks of controlled cooling in elaborate temperature-controlled furnaces gives a low yield of lens blanks meeting specifications. One result is that 193 nm stepper systems have been designed to use the minimum number of CaF_2 lens elements possible, though CaF_2 has not been designed out entirely.

A further unexpected complication from the use of CaF_2 lens elements in 193 and 157 nm lithography systems resulted from a faulty assumption that the cubic crystalline structure of CaF_2 would ensure isotropic- and polarization-independent optical properties (for high-quality crystals), as could be “demonstrated” by naive symmetry arguments and measurements at longer wavelengths. In fact, CaF_2 turned out to have substantial index anisotropy and birefringence at the short wavelengths of 193 and 157 nm.⁸⁸ This is due to the symmetry-breaking effects of the finite photon momentum at these wavelengths, giving rise to a “spatial-dispersion-induced” or “intrinsic” birefringence.⁸⁹ Fortunately, the symmetric nature of this effect has enabled it to be minimized by judiciously orienting the crystal axes of several lens elements to substantially cancel the effects.

Beyond 157 nm, a few shorter wavelengths have been considered for further resolution extension: 126 nm from Ar_2 excimer lasers⁹⁰ and 121.6 nm from hydrogen Lyman- α discharge sources.⁹¹ At these wavelengths, the only transmissive optical materials known are LiF , which has high extrinsic absorption and poor exposure durability, and MgF_2 , which has high natural birefringence due to its noncubic crystal structure. These shorter wavelength technologies have not been developed beyond feasibility studies.^{90,91} Below about 100 nm, no practical material is transparent and refractive optics are not possible. For reasons primarily associated with the development of immersion lithography discussed later, 157 nm lithography, though demonstrated to be technically feasible,⁸⁷ has been dropped off of technology roadmaps.¹⁴ It now appears likely that the shortest wavelength that will be used for production lithography with refractive optics is 193 nm.

As of 2008, 193 nm steppers are the primary tools for producing critical layers of high-volume, leading-edge ICs. Their ArF excimer laser sources are pulsed (≈ 6 kHz, 10 mJ/pulse) and line narrowed (≤ 0.25 pm spectral bandwidth).⁹² The transmission photomasks are made from fused silica with Cr absorbing features and have thin-membrane pellicles to keep uncontrolled particles from collecting on the mask and imaging onto the wafer. The stepper optics are made of fused silica spherical and aspheric lenses, calcium fluoride lenses with clocked crystal axes, mirror elements with aspheric surfaces, and immersion fluids between the last lens element and the wafer, as discussed below.

While the wavelength was progressing down to 193 nm, the other two factors in Equation 19.1, k_1 and NA, were also being pushed towards their limits. A number of resolution enhancement techniques have been used to drive the k_1 factor down to achieve IC structures with half pitches corresponding to a value of k_1 approaching the limiting value of $k_1 = 0.25$.⁹³ Nearly all of these have been taken over from established optical techniques in other fields such as microscopy. These have included (1) illumination methods (off-axis illumination and partial-coherence control), (2) mask modifications to engineer desired wavefronts (phase shift masks, sub-resolution mask structures, and other optical proximity corrections), and (3) resist contrast improvements. For the 45 nm technology node, logic manufacturers are expected to operate with k_1 factors down to about 0.31,⁹⁴ and further extension with k_1 factors down to 0.29 is considered feasible.⁹⁵ Unfortunately, accompanying these gains, process latitudes have been shrinking to marginally tolerable levels. Clearly, k_1 factor improvements for single exposures are nearly tapped out.

The last factor left in Equation 19.1 is the numerical aperture, $\text{NA} = n \sin \theta$. For air between the final lens element and the wafer, the limiting value is $\text{NA} = 1$. The GCA 4800 DSW stepper in 1978 had an NA of 0.28.⁹⁶ The NA has been increased steadily in newer designs by increasing the size and complexity, and consequently the cost of the lens systems. To contain the number and size of lens elements as the NA was increased, the lens system designs had to incorporate aspheric lenses and off-axis mirror elements (catadioptric designs). Further, as the NAs approached 0.9, the polarization effects could no longer be ignored and illumination polarization control became an essential part of the lithography process, further complicating the lithography tools and processes.^{84,97} State-of-the-art dry 193 nm stepper optics have an NA of about 0.93, contain about 30 lenses, with a path length through lens material of about 1 m, and weigh 500 kg or more.¹⁰ With a dry NA limit of 1.0, there is very little possible gain left to justify the vastly increased cost and complexity needed for improvement—an exponential increase in cost for an asymptotic gain. The $\sin \theta$ factor is also essentially tapped out.

Figure 19.10 shows, along with the critical feature size (half pitch), the limiting value of 0.25λ for each wavelength. Clearly, by 2006, the critical feature size 65 nm had approached its limit for 193 or 157 nm. In the 1990s, this projection was the reason why it was nearly universally assumed that alternative technologies, such as EUV lithography, would have to take over below this feature size. This has turned out to be incorrect primarily for two reasons: the NA is not limited to 1 if immersion fluids are included and the effective k_1 factor can be decreased below 0.25 with multiple exposures and processing on the same layer.

19.3.2 193 nm Immersion Lithography

Equation 19.1 is valid at the image plane, which of course must be in the resist. In principle, the $\text{NA} = n \sin \theta$ should be evaluated in the resist, which typically has a 193 nm index in the range

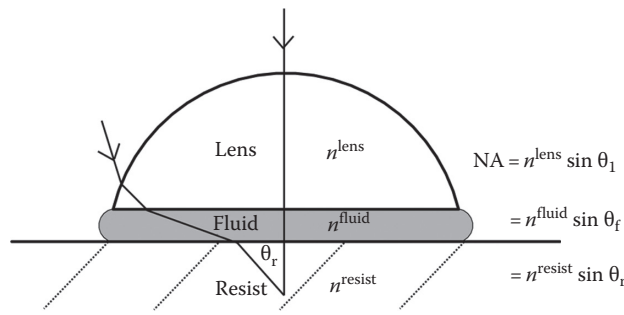


FIGURE 19.11 Schematic of an on-axis ray and a marginal ray through the last elements of an immersion lithography optical system. The angles θ_l , θ_f , and θ_r are the angles of the marginal ray with respect to the surface normal in the lens, fluid, and resist, respectively. For the case shown here, the refractive index of the fluid is less than that of the lens and resist, and n^{fluid} is then the maximum possible NA of the system.

$n = 1.6\text{--}1.7$. However, by Snell's law ($n_1 \sin \theta_1 = n_2 \sin \theta_2$), $\text{NA} = n \sin \theta$ can equally well be evaluated above the resist. Until the recent introduction of the immersion stepper, the space between the final lens element and the wafer was filled with air or N_2 gas, with an index near $n = 1.0$. A consequence is that in spite of the much higher index of the resist, the NA has a maximum value of 1.0. However, as microscopists have known and exploited for centuries, adding a fluid between the image plane and the final lens element allows the maximum NA to be increased.^{98–100} For a planer final lens element, the NA can theoretically be increased up to the lowest index of the resist, the fluid, or the lens, as indicated in Equation 19.4 and Figure 19.11:

$$\text{NA}_{\text{max}} \leq (n^{\text{resist}}, n^{\text{fluid}}, n^{\text{lens}}) \quad (19.4)$$

A nearly ideal immersion fluid for 193 nm lithography turned out to be purified water. It has sufficient transparency at this wavelength, is relatively innocuous to the resist and lens materials, is compatible with resist processing, has low enough viscosity to enable rapid wafer scanning, and is inexpensive. These properties enabled remarkably rapid development and implementation of immersion technology.¹⁰¹ From the inception of substantial 193 nm immersion lithography efforts in late 2002,^{102–105} it took only about 4 years for production-worthy water immersion systems to be built and the process brought into production. Immersion imaging does introduce some new issues, however, including bubble formation in the fluid, evaporation residue defects, resist-immersion fluid interactions, and fluid thermal effects. Polarization effects, already issues for dry systems, have been exacerbated at the extreme NAs of immersion lithography, requiring careful polarization control for differently oriented structures, which puts some restrictions on IC design.¹⁰⁶

With water as the immersion fluid, having a 193 nm index of $n^{\text{water}} = 1.437$, the theoretical minimum half pitch (HP^{min}) for a 193 nm exposure tool decreases to $\text{HP}^{\text{min}} = 0.25 \times 193.4 \text{ nm} / 1.437 = 33.6 \text{ nm}$. Furthermore, at HPs achievable for dry systems, Equations 19.1 and 19.3 show that for the same

HP, the DOF is larger for the immersion approach. Note that the minimum HP for 157 nm dry systems is $\text{HP}^{\text{min}} = 0.25 \times 157.6 \text{ nm} / 1.0 = 39.4 \text{ nm}$, higher than that for 193 nm immersion systems. Attempts were made to identify high-index 157 nm immersion fluids, but only relatively low-index ($n [157 \text{ nm}] \approx 1.35$) fluorocarbon liquids were found to have any practical transparency at 157 nm,¹⁰⁷ and consequently 157 nm lithography technology was dropped from technology roadmaps. As of 2008, water-based 193 nm immersion lithography systems are being operated at an NA in the range of 1.30–1.35 to satisfy the 45 nm technology node with acceptable process latitudes.¹⁴

Approaches to extend 193 nm immersion lithography technology further with higher-index fluids have been pursued. Practical 193 nm transmitting organic fluids with 193 nm indices near $n = 1.65$ (second generation fluids) have been developed.^{108,109} However, the last stepper lens element is made of calcium fluoride with a 193 nm index of $n = 1.50$, or fused silica, with an index of $n = 1.57$. By Equation 19.4, these materials are the bottlenecks for resolution extension. Thus, significant NA gain from higher-index fluids requires higher-index last lens materials as well. Higher-index UV lens materials have been explored for this purpose. Key practical materials identified include $\text{Lu}_3\text{A}_5\text{O}_{12}$ (LuAG) [$n = 2.21$] and polycrystalline MgAl_2O_4 (ceramic spinel) [$n = 1.93$].¹¹⁰ LuAG has the highest index, but efforts have not yet succeeded in improving the 193 nm transmission to the specifications, which are stringent due to its high thermo-optic coefficient, dn/dT . Also, the large value of the intrinsic birefringence for this material is difficult to compensate for. Ceramic spinel solves this problem with its polycrystalline structure, but the polycrystalline nature also results in a high degree of scattering. A further possible high-index lens material being considered is $\alpha\text{-Al}_2\text{O}_3$ (crystalline sapphire) [$n = 1.92$]. Its large natural birefringence due to its uniaxial crystal structure has limited its use in precision optics. However, with its crystal optic axis oriented along the optical axis of the system and with the polarization of all rays arranged to be oriented perpendicular to this axis, a sapphire last lens element could be manageable. As of this writing, LuAG is considered the most promising high-index lens material candidate,¹¹¹ and the industry is still considering whether the practical NA gain to about 1.50 is worth the development effort.

If a third-generation immersion fluid with an index near or above $n = 1.80$ could be developed, then an NA increase to near $\text{NA} \approx 1.7$ could provide enough incentive to justify the substantial development effort required to implement it, because this would enable the 32 nm half-pitch technology node. Pure organic fluids with indices this high cannot have practical 193 nm transmissions. However, the indices of the fluids could in principle be increased to this level by loading the liquids with approximately (2–10) nanometer-size suspended particles of high-index oxide crystals, e.g., HfO_2 or LuAG, while maintaining acceptable transmission, scattering levels, and viscosities.^{112–114} This approach is being explored, but it is regarded at best as complementary to multiple patterning approaches to resolution extension discussed next.

19.3.3 Double Patterning

The process-dependent k_1 factor has been driven down to near the hard limit of $k_1 = 0.25$ for single exposures. However, for multiple exposures and processing steps on the same layer, structures with half pitches corresponding to lower effective k_1 values are possible. A number of these multiple patterning approaches are now being pursued and these are expected to satisfy the requirements for the 32 nm half-pitch technology node and possibly the 22 nm node and below. These approaches differ by the number and sequence of exposure and processing steps used to achieve the desired features. Four basic types are illustrated schematically in Figure 19.12.¹⁴ They all use the fact that while the structure pitch created by a single exposure is limited by diffraction, as characterized by Equation 19.1, processing can be used to tailor the line/space ratios in each period, and subsequent exposure and/or processing steps can interleave further structures to increase the structure density. In the Litho-Etch-Litho-Etch process, Figure 19.12a, two Litho-Etch processes are done in sequence with the second process shifted by half the period to give a pitch doubling. This general process can be used to create arbitrary structures with the half pitch shrunk by a factor of 2 below the diffraction limit, though this scale shrink requires tighter tolerances on line edge control and overlay, among other issues.

A serious difficulty with this process is that it requires that the wafer be taken out of the stepper track for etching and then realigned before the second exposure, creating overlay challenges and decreasing the throughput for the layer by a factor of about 2. A preferred approach would have the two exposures done in sequence with just one etch step at the end: Litho-Litho-Etch, shown in Figure 19.12b. Unfortunately, it can be shown that for a resist system with a linear dose response, as has been universal in DUV lithography, two exposures cannot generate patterns with pitches below the diffraction limit. However, with a nonlinear dose response system, this is possible. A number of nonlinear response approaches are being pursued, including contrast enhancement layers, 2-photon resists, and positive and negative-tone threshold resists.¹¹⁵ One version, Litho-Freeze-Litho-Etch, shown in Figure 19.12c, is particularly promising.¹¹⁶ In this approach, the latent image captured in the resist from the first exposure is “frozen” by chemical treatment. The first frozen image region is protected from any photo response to a second exposure, then a single etch step can create the pitch-doubled structures.

A different approach, known as side wall (or spacer assist) double patterning, requires only one exposure step to create pitch doubling.¹¹⁷ As illustrated in Figure 19.12d, the first exposure and development step is only to create sidewalls at the desired positions. A subsequent thin-film deposition on the sidewalls, chemical-mechanical polishing (CMP) to split the deposited structure,

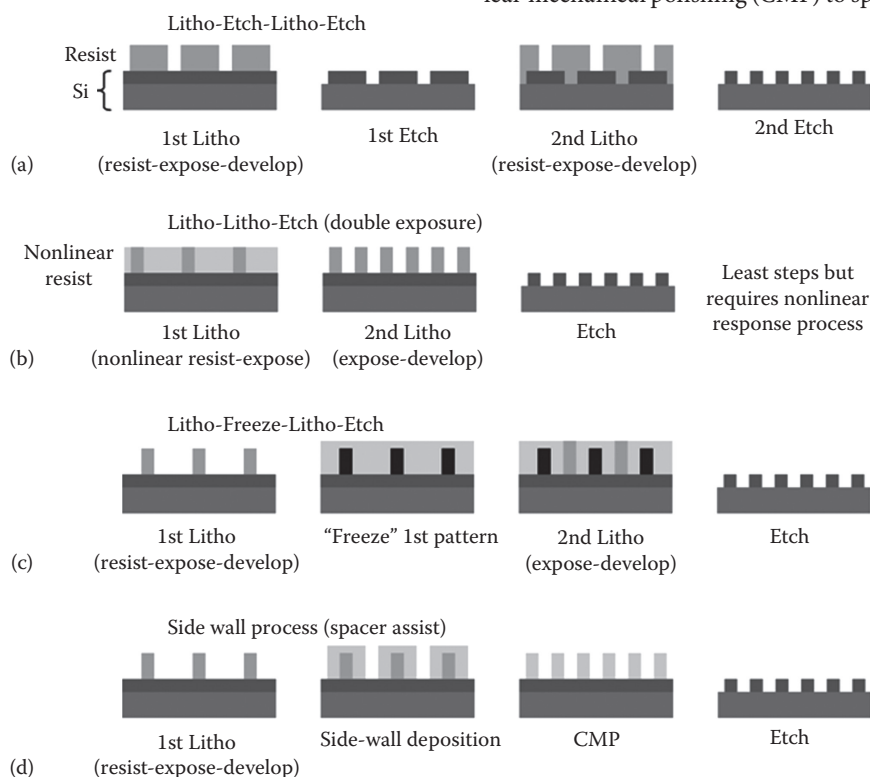


FIGURE 19.12 Double patterning approaches: (a) Litho-etch-litho-etch requires 2 exposures and 2 etch steps. (b) Litho-litho-etch (or double exposure) requires 2 exposures and only one etch step, but needs a resist process with a nonlinear dose response. (c) Litho-freeze-litho-etch has intermediate complexity, requiring 2 exposures, a chemical freezing process after the first exposure, and one etch step. (d) Side wall process (spacer assist) requires one exposure and one etch. It uses side wall deposition and chemical-mechanical polishing (CMP) to achieve doubled pitch.

and elimination of the original pattern enables the desired pitch doubled structures. This approach takes advantage of the well-understood and highly controllable thin-film-deposition technology to obtain the desired linewidths, independent of diffraction limits. Furthermore, the sidewall-derived structures are automatically self-aligned by the original structure. A difficulty with this approach is that restriction to patterning along sidewalls makes design layout much more difficult, and not all structures are topologically possible with single exposures. At least a further exposure/processing step is generally required for arbitrary structures. Still, this method is inherently extendable, and pitch quadrupling, etc. is possible in principle.

19.3.4 Ultimate Resolution Limits of DUV Lithography

Double patterning methods are already being used in IC production, and they are the declared technology solutions, using 193 nm water immersion tools, for several volume semiconductor manufacturers for the 32 nm half-pitch technology node projected for about 2013.¹⁴ These approaches appear feasible for further resolution shrinking as well, e.g., the 22 nm half-pitch technology node. Redesign of 193 nm immersion steppers with high-index fluids and lens materials, in combination with double patterning techniques, offer the potential for further resolution extension and relaxation of the k_1 factor for a given resolution. When double patterning becomes routine, consideration of triple patterning, quadruple patterning, etc. may become tempting. However, this would likely have to come at the cost of much tighter process control requirements, such as CD and overlay control, than is presently attainable. Improvements to meet the requirements, along with the increased complexity (more exposures and processing steps per layer) will surely drive up costs substantially. There is little doubt that these DUV lithography extension approaches can be made to work technically. It is just a matter of whether they can operate at commercially viable costs and whether any reliable alternatives can be implemented at less cost. For example, rapidly increasing mask costs have made the numerous maskless technologies, such as multi electron-beam direct write schemes, very attractive, at least for low-volume production.

For high-volume leading-edge ICs, it is generally agreed that for the 22 nm half-pitch technology node and below, a reliable single-exposure EUV solution, with its larger depth of focus and more natural extendibility, would be preferred. However, formidable challenges, repeated introduction delays, and especially rapidly rising projected costs, have made this solution not so inevitable as it once seemed at the beginning of the decade. Cost is the ultimate driver. If or when DUV lithography is displaced, and what its ultimate practical resolution limits are, is now less clear than ever. The technology has thrived on remarkable innovativeness and resourcefulness and its development history does not suggest that these will cease. Previous predictions of its limits and of its imminent replacement have always been wrong.

19.4 Electron-Beam Lithography

Electron-beam lithography has demonstrated its utility over several decades as both a primary pattern generation tool for the semiconductor industry and as the premiere means of patterning small structures for advanced device development and research in myriad fields. Like any lithographic technology, its suitability for a given application depends on its performance with respect to the four metrics of resolution, throughput, pattern placement, and cost-of-ownership. As we shall see in the following sections, electron-beam systems excel with respect to resolution and pattern placement, but suffer from fundamental limits in terms of throughput.

19.4.1 Resolution

Resolution in a lithographic process is a rather ill-defined quantity since, by virtue of the fact that it is a process involving many steps, a large number of variables are involved. These can frequently be manipulated to produce isolated features far smaller than might, at first sight, be judged possible. The true test of the process is the minimum pitch of the features that can be fabricated. In what follows, we will consider primarily those factors that are unique to electron-beam exposure and neglect those that are common across the various exposure techniques—those are covered elsewhere in this chapter.

The ultimate resolution that can be obtained using electron-beam exposure is determined by the nature of the interactions of the electrons with the material being exposed. There are two parts to be considered: first, the trajectories that the incident, or primary, electrons follow within the material and second, the processes by which the energy deposited by the primary electrons is translated into developable chemistry in the exposed material.

The electron trajectories are determined by the combination of incident electron energy and resist/substrate atomic number.^{118,119} At low energies/high atomic numbers, the electrons scatter strongly within the solid, which leads to substantial broadening of the beam as it penetrates the material. Since most resist materials are organic, their average atomic numbers are not dissimilar from that of carbon, so the beam broadening, or forward scattering in the resist, is determined principally by the electron energy. For this reason, most high-resolution systems operate at energies of 50–100 keV. In addition, because the beam broadening increases progressively as the electrons undergo additional elastic scattering events on their way through the resist, thin resists yield higher resolution images. Very low (<500 eV) incident energies have also been proposed as a means of generating high-resolution images.^{120–122} In this case, the beam broadening is on the order of and constrained by the very short total range of the electrons within the resist. The resist thickness is therefore limited to that range, which may be insufficient for subsequent processing needs, and the resolution can only be improved by reducing the energy (and the resist thickness) to impractically small values.

The incident electron energy, E_0 , has a dramatic impact on the dose needed to expose resist, which, for energies above about 5 keV, varies linearly with E_0 . This is a reflection of how the inelastic scattering cross section varies with electron energy. The effect is captured by the Bethe continuous slowing-down approximation¹²³ that describes the average rate at which fast electrons lose energy along their trajectories. At high energies and resist thicknesses that are small relative to the electron range, the feature width is determined not by the deviations in the trajectories of the primary electrons due to elastic scattering, but by the volume in which they deposit energy. Although the primary electrons can cause chemical changes in the resist directly, it is normally assumed that the so-called fast secondary electrons generated by inelastic scattering of the primary beam are responsible for the majority of broken bonds in the resist.¹²⁴ This is because the low-energy secondary electrons have a much larger interaction cross section than those of the primary beam.¹¹⁸ Conceptually, each primary electron trajectory can be thought of as surrounded by a cylinder of material 10–20 nm in diameter exposed by the secondaries that it generates. At very low incident electron energies, the stopping power increases significantly and the electrons deposit all their energy efficiently in the resist film, rather than carrying on through to the substrate.¹²⁵

The resolution that can be achieved in a resist can also be estimated by considering the impact parameter for energy-loss events for the primary electrons. An electron traveling with velocity v , interacting with a stationary electron at a distance b delivers an impulse having a duration of approximately b/v and contains frequency components, ω , up to v/b . These correspond to a maximum energy transfer, ΔE , of $h\omega/2\pi$.^{126,127} For 100 kV electrons and ΔE s of 5, 50, and 500 eV, b is 10, 1, and 0.1 nm, respectively. Normally, the energy scale relevant to resist exposure is on the order of a few electron volts (3.6 eV for the C–C bond), leading to an interaction distance of a few nanometers but in a few cases the energy needed is much higher, corresponding to a core-shell excitation, for example. In systems such as alkali metal halides, in which the exposure mechanism depends on the dissociation of the halide ions from the lattice, resolutions of 1–2 nm are achievable.^{128–130} Unfortunately, the doses required are in the C/cm² range, which is not practical for manufacturing. Currently, the highest resolution material that is suitable for nanofabrication is hydrogen silsesquioxane (HSQ), which has demonstrated feature sizes as small as 7 nm half-pitch.¹³¹ This is an inorganic, small-molecule resist that essentially forms silica upon exposure and development. Its increased mechanical strength relative to organic resist materials is one reason for its ability to produce small features, while its higher average atomic number may help reduce the range of the fast secondaries, contributing to its high resolution.

Electron–solid interactions also affect the resolution in electron-beam systems through the proximity effect. This is the additional exposure of the resist by electrons backscattered from the substrate and it leads to a loss in contrast and thus to a loss in resolution. At higher voltages and on low-atomic number

substrates (e.g., Si or SiO₂), the backscattered electrons have a relatively large range ($\propto V^{5/3}$) and the contribution of the forward and backscattered electron doses can be captured by the two-Gaussian model¹³²

$$D = D_0 \left[e^{-x^2/\alpha^2} + \eta e^{-x^2/\beta^2} \right] \quad (19.5)$$

where

D_0 is the incident dose

α is the width of the forward-scattering distribution

β is the width of the backscattered distribution

η is the effective dose contributed by the backscattered electrons

As we have discussed above, α is typically on the order of 10 nm, while β is on the order of micrometers. η can be quite large, depending on the substrate's atomic number and is approximately 0.5 for Si at 100 kV.¹³³ This model is applicable if the forward and backscattered dose distributions can be readily separated. In this case, small, isolated features receive a dose of D_0 , the centers of large features receive a dose of $D_0(1 + \eta)$, and all other types of features receive a pattern-density dependent dose that varies between those values. As long as the feature size is small compared with β , this dose variation can be corrected for either by adjusting the dose delivered to individual features,¹³⁴ applying the inverse of the background dose to produce a flat background,^{135,136} or adjusting the size of the features^{137,138} by using a pattern density averaged over a length scale on the order of β . However, if either α or β approach the feature size, then much more computationally intensive techniques must be used to perform an iterative correction procedure, as the correction applied to each feature affects its neighbor and vice versa.¹³⁹ At low energies and in high atomic number substrates such as GaAs or InP, the deposited energy distribution is more complex^{140,141} and the proximity effect becomes much more difficult to correct. It is, however, important to point out that these phenomena are analogous to the flare and optical proximity effects encountered in advanced optical lithography, for which correction techniques are at an advanced stage of development.

So far in our discussion, we have implicitly assumed an ideal point source of electrons incident upon the resist. A close approximation can be achieved in practice with low-current, focused probes in electron microscopes. However, for practical applications, we need high beam currents, and this has a dramatic impact on the design and operation of electron-beam lithography tools and leads to systems in which the intrinsic resolution of the resist and process is often better than that of the electron optics.

19.4.2 Throughput

In the design of most optical systems, including electron microscopes, there is a trade-off between blur due to diffraction, which scales as $1/NA$, where NA is the numerical aperture of

the system, and aberrations that generally scale as some power of NA (a spherical aberration is often a dominant term and varies as NA^3). In electron-beam lithography systems, throughput is critical to their cost of ownership and ultimate utility. Unlike photons in a light-optical system, the electrons in an electron-optical system affect one another strongly through unscreened Coulomb repulsion. The interactions give rise to three principal effects: (1) the forces between electrons along the electron-optical axis lead to the speeding up or slowing down of individual electrons, which is equivalent to an energy spread in the beam, known as the Boersch effect; (2) the average force due to all the other electrons in the beam leads to deterministic changes in electron trajectories and leads, to first order, to an overall defocusing of the beam, known as the global space-charge effect; and (3) the interactions between individual electrons lead to random changes in individual electron trajectories, known as the stochastic space-charge effect. The severity of the Boersch effect depends on the chromatic aberration in the system. The global space-charge effect can be thought of as creating a negative lens in the system whose effects can be compensated for by refocusing the beam. However, if the current density is not uniform across the beam, that lens becomes highly aberrated and its effects cannot be compensated. The stochastic space-charge effect is not correctable. As might be expected, the space-charge effects are made worse when the electrons are forced closer together or can interact for longer periods and increase with beam current, I , and column length, L , and are mitigated when the electrons are spread farther apart or interact for shorter times and decrease with increasing numerical aperture α , the demagnification factor, M , and the accelerating voltage, V . The detailed dependence of beam blur on I , L , V , M , and α is particular to a given system and has been studied in depth for both single-column, probe-forming,¹⁴² and projection systems.^{143,144} Note that improvements realized by increasing the voltage are offset by the need to increase the beam current to compensate for the linear decrease in resist sensitivity with voltage.

The net result of these effects is that rather than balancing diffraction and aberration blurs, the system optimization must be performed by balancing space-charge and aberration blurs. This means that for any given beam current in a system, there is an optimum numerical aperture that must be used and a corresponding minimum blur that can be achieved. Any attempt to increase the beam current leads to an increase in beam blur. Electron-beam lithography systems for nanofabrication research are generally designed to provide the optimum resolution, with throughput as an important, but secondary goal. However, the semiconductor industry's continuing demand for ever-smaller features and higher throughputs has resulted in the disappearance of electron-beam lithography from the direct IC fabrication process because of the conflict between the need for increased beam currents to increase throughput and the need for the decreased beam currents necessary for improving resolution cannot be resolved at the feature sizes now required.

In the future, the throughput of electron-beam lithography, even for mask making, is likely to become worse. To understand why this is the case, it is necessary to examine how resist sensitivity scales with feature size.

If we consider a feature of CD L and allow it to vary by no more than $L/10$, then we can define an image pixel as $L/10 \times L/10$. In order for each pixel to be faithfully reproduced, we need the resist to be able to clearly distinguish between exposed and unexposed pixels. Even if the dose over a large area is fixed at a precise value, the arrival of the electrons at any pixel is a statistical process, with the number of electrons delivered following a Poisson distribution. This effect is frequently referred to as shot noise and has been extensively studied.¹⁴⁵⁻¹⁴⁹ We can, therefore, define a minimum number, n , of electrons per pixel that is necessary to ensure that the error rate of improperly exposed pixels is suitably small. The total dose needed per unit area therefore becomes $100n/L^2$, i.e., it scales as $1/L^2$, and the beam current necessary to maintain a given real exposure rate must therefore scale in the same fashion.

19.4.3 Overlay

The fact that magnetic and electric fields can deflect electrons precisely and at high speed is one of the great strengths of electron-beam systems. In optical lithography systems, accurate and precise registration and overlay can only be achieved by ensuring nanometer-scale mechanical alignment between mask and wafer stages—physically massive systems that can only be controlled with bandwidths of a few tens of Hz. In electron-beam tools, it is not necessary to control the stage precisely (offsets of several micrometers between the actual and planned stage coordinates are common), because the position of the electron beam can be adjusted, at speeds of up to 100 kHz, to make up the difference, provided a suitable signal from the stage interferometers is available. There are generally differences in the coordinate system that are generated by the stage and the substrate. Normally, these are accounted for by periodically acquiring alignment mark information from the substrate. This procedure is susceptible to errors arising from drift occurring between mark measurements and schemes have been developed that enable registration data to be generated from the substrate continuously.¹⁵⁰ The ability to adjust the position of the beam, as well as characteristics such as focus and stigmatism, in real time, makes it possible to correct for a large variety of errors, such as those caused by variations in substrate height. Along with the benefits it brings, the sensitivity to fields is also a source of difficulty associated with electron-beam systems: interference from dynamic fields must be reduced as far as possible, while that from static ones, such as those due to the small magnetic inhomogeneities of the stage, must be carefully mapped and calibrated out.

Another source of error peculiar to electron-beam tools, particularly at high voltages, is substrate heating. The total amount of energy deposited in the substrate scales as the square of the accelerating voltage because of the combination of the

increasing energy per electron and the increasing resist dose required. The concomitant substrate heating can affect both pattern placement/overlay, as a result of thermal expansion,¹⁵¹ and CD control, as resist sensitivity may vary with temperature.¹⁵² Temperature increases are more severe in SiO₂ substrates because of silica's poor thermal conductivity, while Si substrates, with their higher coefficient of thermal expansion, are liable to greater placement errors.

19.4.4 Cost of Ownership

As we have seen, although electron-beam systems provided exceptional resolution, and are capable of precise pattern placement,¹⁵³ they are fundamentally limited in throughput. Historically, for relatively large feature sizes, the limiting factor in throughput was the serial nature of the writing process in probe-forming, or Gaussian-beam, systems and this led to the development of schemes such as shaped-beam,¹⁵⁴ cell-projection,¹⁵⁵ large-area,^{6,156} and full-field projection¹⁵⁷ that sought to deliver more than one pixel's worth of information at a time. Unfortunately, as feature sizes decreased and the resolution requirements became more demanding, they all ran into space-charge limits. This has relegated electron-beam systems for production purposes to the fabrication of small numbers of high-value items such as photomasks, CD/DVD masters, and nanoimprint templates. There are two routes out of this dilemma: the first is to accept the limited throughput, but use the essential addressability of electron beams to create flexible systems—maskless lithography tools—that can create ICs without the need for masks and their associated costs;^{158,159} the second is to avoid the space-charge limits of single columns by dividing and conquering—using multiple small columns to keep the electrons far enough apart so that their interactions are insignificant.^{160,161} In the first case, the cost of ownership is competitive with photolithography for short-production run devices where only a few wafers worth of devices are produced for each mask set. In the second case, providing that issues associated with source uniformity, control, and brightness can be overcome, then it may be possible to have the best of both worlds—flexibility in patterning together with high throughput—making it directly competitive with optical lithography. Research and development are active in both areas.

19.5 Nanoimprint Lithography

Nanoimprint lithography (NIL) is rapidly emerging as a low-cost, high-resolution, and versatile alternative to optical lithography as a patterning technology for semiconductor fabrication and other applications that incorporate nanoelectronic devices.^{162,163} Optical lithographic techniques, including state-of-the-art tools based on 193 nm radiation⁹⁸ or next-generation potential solutions, including extreme ultraviolet (EUV, 13.5 nm radiation) lithography,^{164–166} rely upon selectively exposing a photoactive film to radiation via a photomask that defines the lithographic pattern of interest. A chemical reaction occurs in the exposed

regions of the film that renders them soluble in an aqueous base, creating a physical pattern defined by the unexposed regions in the film. It is becoming increasingly difficult to control the resolution of this patterning process.

NIL offers a potentially simplified alternative to chemically amplified resists. All NIL techniques rely on a simple squeeze-flow mechanism whereby a resist flows into a well-defined physical cavity of nanoscale dimensions. It is a molding or replication technique where the ultimate resolution is defined by the physical dimensions of the imprint mold cavities.^{167–170} If high-resolution masters can be created, high-resolution copies can be generated. It is also a repetitive stamping or replication technique. The well-defined patterns in the imprint master can be used to create thousands of replicas, analogous to how the metallic master for an LP record were used to stamp thousands of inexpensive vinyl copies for consumer use. Compared with optical lithography for high-volume nanomanufacturing, there is an important distinction worth highlighting. With optical lithography, every printing or copy of the nanostructured surface requires extremely tight control of the environmental conditions to maintain the sensitive balance of the complicated reaction, diffusion, and dissolution process for the chemically amplified resists.¹⁷¹ This is precisely why state-of-the-art optical lithography tools cost upwards of \$30 M apiece, providing a 65 nm patterning resolution, and semiconductor fabrication lines cost billions of dollars to construct.

The resolution of NIL is largely controlled by a simple squeeze-flow process.^{167–170} As long as high-quality, high-resolution imprint masters can be fabricated, it is relatively easy to stamp out copies of the mold. In optical lithography, the ultimate patterning resolution is intrinsically coupled with the high volume manufacturing process making process control measures extremely important. Every single copy manufactured requires stringent control over the reaction, diffusion, and dissolution processes. With NIL, the resolution is less coupled with the high-volume manufacturing process and more dependent on the mold or imprint master fabrication. For these reasons, NIL tools tend to be significantly less expensive. Research and development grade imprint tools can be purchased for about \$100 K, while manufacturing grade tools cost approximately \$2 M, both with a sub 10 nm resolution.

Both optical and nanoimprint lithography are dependent on high-resolution masks or masters. In optical lithography, the mask sets required to fabricate a semiconductor device can cost several millions of dollars to produce, comprising a significant fraction of the manufacturing costs. These are phase-shifting optical masks in which blanket UV radiation is exposed to one side, generating selectively exposed regions in the resist film on the other side. This exposure is also done through a series of lenses where the features in the mask are approximately four times larger than the image at the wafer plane. In NIL, these mask costs are likely to increase. The squeeze-flow is a direct write process where the features in the mold are the same size as the features in the wafer plane; there is no longer this 4x reduction. This means that high-resolution and costly electron-beam

lithography is needed to fabricate the imprint masks, compared with optical lithography where the mask resolution requirements are somewhat reduced because of the lens system. There are no lenses in NIL and the imprint masks may very well be more costly to produce. Furthermore, these expensive NIL mask sets must be mechanically pressed into the resist film. In optical lithography, the masks are isolated from the resist behind a transparent and protective pellicle. There are no protective pellicles in NIL and one must make direct mechanical contact of the expensive mask with the resist film.

In this section, we provide a general overview of the NIL technology. Our discussion will be largely limited to the field of nanoelectronics, including complementary metal-oxide semiconductor (CMOS) devices, although NIL is also widely considered to be a manufacturing alternative for several other forms of nanotechnology. We will elaborate on the differences between NIL and existing optical lithography techniques and discuss some of the unique materials and metrology challenges that NIL processes introduce. We will also provide a brief overview of some of the recent developments in applying NIL to nanoelectronics technologies.

19.5.1 Variations of NIL

19.5.1.1 Thermal NIL

NIL generically refers to pressing a hard mold or template decorated with nanoscale patterns into a softer material to lithographically define well-controlled nanostructures.¹⁶⁷⁻¹⁷⁰ In most cases, pattern formation is accomplished by a squeeze-flow mechanism whereby the material flows into the mold in a liquid-like state (Figure 19.13). Of course, this requires

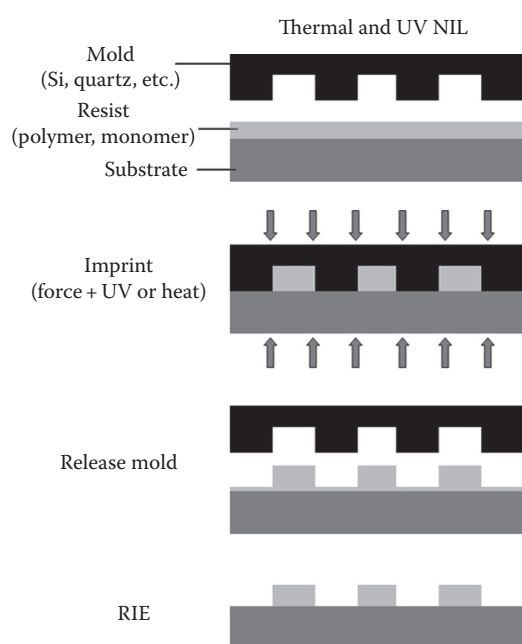


FIGURE 19.13 Schematic of the NIL process, showing both the thermal and UV forms.

“setting” the pattern in the liquid material. In the thermal embossing form of NIL, the resist is typically a glassy polymer.^{167,168} During the imprint process, the film and the imprint mold are heated to above the glass transition of the polymer while applying an external pressure. Under elevated pressure and temperature, the polymer flows into the cavities of the mold. The pattern is set by cooling the system to below the glass transition of the polymer, where the material vitrifies into a rigid glass. When the mold is separated from the substrate, the surface is left with nanoscale patterns that are relief images of the mold cavities. A cavity in the mold becomes a polymeric pattern on the surface.

The thermal embossing form of NIL is similar in concept to many of the bulk molding or forming processes used to manufacture large scale plastic components. High molecular mass polymers, even at temperatures far above their glass transition, tend to be high viscosity fluids. Flow does not always readily occur under quiescent conditions meaning that pressures must be applied to squeeze the material into the mold. Most NIL tools designed for thermal embossing are capable of applying pressure as high as 5 MPa. This is combined with maximum temperatures of typically 200°C to 300°C, which means that most tools are capable of exceeding the rubbery plateau modulus for most polymer melts and able to induce material flow.

There are several different options when it comes to applying the heat and pressure for thermal NIL. One class of tools is largely based on the photomask aligner and wafer bonding systems widely used in the semiconductor industry. In many instances, an imprint module can be purchased as an add-on for an existing tool. In these systems, mechanical platens with heating elements are used to apply the temperature and pressure to the imprint mold and substrate. Their advantages are that they provide uniform heating through the large thermal mass of the platens and they often have a built-in capability for optical overlay alignment between the imprint mold and the substrate. The primary disadvantage is that maintaining parallel contact between the platens can be difficult. Misalignment of just a few μm can prevent conformal contact, which makes it very difficult to imprint nanoscale features over large areas. To overcome the conformal contact issues, some imprint tools utilize hydrostatic gas pressure to squeeze the imprint mold into the resist film.¹⁷² This pressure is applied through what is essentially a deformable gas bladder. Since the NIL molds or masters are usually etched into thin Si or quartz wafers and imprinted onto similar thin Si substrates, the molds and wafers are able to bend or flex to a certain extent and increase the degree of conformal contact. In some tools, the pressure is applied through the top through the gas bladder while the substrate rests on a rigid metallic platen that provides the heating. These systems provide an optimal balance between uniform heating and conformal contact. There are also tools that utilize an entirely soft press technology, where pressure is applied through both the top and bottom through deformable gas bladders. In these cases, the bladders are transparent and the heating of the substrate is provided through infrared heat lamps. This soft press technology maximizes the pressure uniformity

across the mold and substrate while the reduced thermal mass (no platens) allows for rapid heating and cooling rates. However, the noncontact optical heating means that temperature uniformity and stability are more difficult to achieve.

19.5.1.2 UV NIL

One disadvantage of thermal NIL is that it requires heating and applying pressure to the substrate. For certain applications, the patterned substrate may or may not be able to withstand the thermal budget associated with this process. Likewise, large temperature changes can induce thermal distortions, which make overlay and alignment difficult. UV NIL offers a low temperature alternative to thermal NIL. In UV NIL, the resist is a liquid-like (or low viscosity) monomer that readily flows into the mold cavities at room temperature with no heating and very little pressure.^{169,170} In many instances, the liquid monomer is actually wicked into the mold via capillary forces, minimizing distortions of the substrate or the template (Figure 19.13). In the mold, the monomer undergoes a cross-linking reaction upon exposure to UV radiation, creating a hard glassy pattern that retains its shape after separating the mold from the substrate. This means that either the NIL mold or the supporting substrate must be transparent to the appropriate UV radiation. For this reason, the molds are typically fabricated in quartz wafers, whereas silicon and nickel are more common materials in thermal NIL. An additional requirement is that UV NIL is limited to patterning materials that cross-link under UV radiation. Thermal NIL can, in principle, be applied to any material in which flow can be induced.

19.5.1.3 Transfer Printing

Both the thermal and UV forms of NIL described thus far are similar to optical lithography in that a pattern is created in a resist film that has been previously deposited on the substrate of interest. It is also possible to employ the NIL technologies in a material transfer mode that is similar to most industrial forms of printing. In transfer printing, the material that is to be patterned is first applied to a patterned stamp or mold and then transferred via mechanical contact to the target substrate. This requires tuning of the differential adhesion between the pattern mold and the substrate such that the material adheres to the substrate more strongly than the patterned mold. There are two primary modes in which transfer printing can occur¹⁷³ (Figure 19.14). The first is a whole layer transfer where a continuous film with a nanoscale texture defined by the mold topology is transferred to the substrate. The second is a discrete transfer or inking mode where material is selectively transferred to the substrate from the protrusions of the mold; any material in the cavities of the mold is not transferred over. Whole layer transfer is used primarily to create topological patterns of a given material on the target substrate. Examples of this technology are being used to create nano- or microfluidic channels or devices. The discrete transfer mode can also be used to create physical patterns, but it also has the ability to create chemical patterns of a given surface energy or chemical functionality by essentially inking monolayers of a

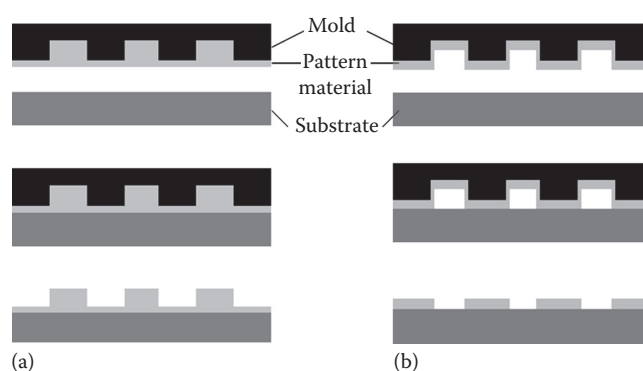


FIGURE 19.14 Schematic of two modes of transfer printing: (a) whole-layer transfer and (b) inking.

chemical compound. In this last case, the pattern may, to a first approximation, lack topology and not alter the smooth surface of the substrate. Chemical patterns like these are commonly considered in sensor-type applications.

19.5.1.4 Functional Materials

One of the biggest distinctions between NIL and competing optical lithography methods is rooted in the generality of the patterning process. In nearly all forms, optical lithography focuses on creating high-resolution patterns in sacrificial photoresist formulations. As mentioned previously, photoresists are highly complicated materials systems that balance chemical reactivity, acid diffusivity, and their dissolution behavior to optimize their patterning resolution. Once the pattern is formed, the resist becomes a sacrificial component for subsequent additive or subtractive processes to transfer the pattern into the functional materials of interest. On the contrary, the mechanical stamping and squeeze-flow processes used in NIL are generic mechanisms applicable to a wide range of materials. This means that a wide range of materials can be patterned directly by NIL, including functional materials. The resolution of NIL processes is controlled by the mold or mask fabrication process more so than optical lithography. The ability to directly stamp nanoscale structures into functional materials is a highly attractive way to simplify the number of parameters impacting patterning resolution, reduce the number of nanofabrication steps, and thereby reduce manufacturing costs.¹⁷⁴

19.5.1.5 Tool Types

NIL is a low-cost nanopatterning alternative to optical lithography with the potential for high-volume manufacturability. Mechanical stamping processes have a long history in manufacturing environments and the same appears to be bearing true for the emerging field of nanomanufacturing. Stamping processes are intrinsically compatible with manufacturing assembly lines. However, NIL is still in its infancy period and most of the tools that are commercially available today are geared for R&D or the technology development. There are examples of high-throughput tools in the market, but most of

the activity is still in the lab as opposed to pre-production. In this section, we review the different types of tools with respect to patterning throughput.

The most versatile tools on the market today also have the lowest throughput and least applicability for high volume nanofabrication. These account for most of the imprint tools sold today from companies like Nanonex, Obducat, or Jenoptik that utilize gas pressure through some type of deformable bladder to apply a very uniform pressure to the mold and the substrate. Typically, these tools are very flexible and provide the user with a wide variety of process control, at the sacrifice of throughput. The user has the freedom to place an arbitrary mold onto an arbitrary substrate, sandwiched between one or two sheets of deformable rubber or foil. This stack is then placed inside a movable gas chamber. The gas chamber closes down on the deformable bladders, creating pressure reservoirs on the top and/or bottom of the sample. A vacuum pumping system is also usually involved to evacuate the sample region between the bladders. Nitrogen or some other inert gas is then pumped into the chamber, generating pressures as high as approximately 5 MPa to press the mold into the substrate. Heat is then applied through either the optical heat lamps or thermal sample block to enable flow of the material into the mold cavity. After a prescribed heating cycle of a few minutes, the temperature is cooled back to room temperature and gas chambers are vented to release the pressure. The sample and the mold are then manually removed from the chamber and manually separated to reveal the patterned substrate. This process obviously describes the thermal form of NIL. The same general process applies for UV NIL with these tools with the exception that lower pressure is required and UV radiation is applied instead of heat. In either case, UV or NIL, these single stamp tools are capable of generating one patterned substrate approximately every 10–15 minutes with manual input from the user. For most applications, this throughput is not suitable for manufacturing. Rather they are designed for flexibility and ease of use. The sample chambers typically vary from approximately 5–20 cm in diameter and allow arbitrary form factors or piece parts to be imprinted. This is primarily useful for technology development. One notable exception is a large area single imprint tool being developed at the Korean Institute of Machinery and Materials.¹⁷⁵ This is a low pressure UV imprint tool capable of imprinting an entire 45 cm (diagonal) flat panel display uniformly in a single imprint. Cycle times of 4–5 minutes here would probably be more acceptable given the limited demand for such high-end displays. These cycle times would be totally unacceptable for the high volume demand of bit patterned magnetic media for data storage hard drives.

There are efforts to increase the throughput of imprinting tools. The next class of tools generically utilizes a stamp and repeat technology to generate multiple copies of a single pattern across a large substrate. This form of stamp or step and repeat technology is naturally compatible with the form factor of multiple dies (or devices) per wafer that is currently used in semiconductor fabrication.¹⁷⁰ So these types of tools tend to be targeted

for CMOS devices. Molecular Imprints, Inc. is the pioneer in developing step and repeat tools, although other companies including EV Group and Nanonex now offer tools with similar capabilities. Throughput or manufacturability tends to be the primary driver for going from a single imprint to a step and repeat tool. For this reason, most step and repeat tools are based on the UV NIL process, which is usually faster because it lacks the heating and cooling cycles associated with thermal NIL. Furthermore, locally heating a selected region for imprinting on a larger wafer or substrate is difficult. It is much easier and faster to locally expose the imprinted region to UV radiation. Lastly, these step and repeat tools are usually optimized for throughput that comes at the price of the flexibility in the patterning processes or conditions. The general use single imprint tools typically offer greater flexibility. For example, single imprint tools are usually capable of performing either UV or thermal NIL on a variety of materials whereas step and repeat tools tend to be limited to UV NIL patterning of a given resist formulation that has been optimized for the system.

The NIL tools discussed thus far have largely been designed as drop-in replacement technologies for optical lithography, with the target applications in CMOS. However, there have been recent advances in building roll-to-roll NIL tools that are capable of patterning continuous sheets or strips of a nanopatterned substrate.^{176,177} Roll-to-roll processes are capable of generating patterned media at a rate at least several orders of magnitude faster than traditional optical lithography, enabling high volume nanofabrication. However, roll-to-roll processes tend to provide very poor overlay capabilities, practically limiting the advantages to single-layer devices. For these reasons, the target applications migrate away from CMOS to emerging markets where nanopatterning has yet to be realized. Examples might include antifouling biological films, polarizing or anti-reflective optical coatings,¹⁷⁸ brightness enhancing films for large area displays, or flexible electronic devices like radio frequency ID tags.¹⁷⁹ In the roll-to-roll form of NIL, the mold cavities are fabricated onto either a circular drum or a tractor tread-like device. A continuous film is fed in between a pair of rollers that rotate in opposite directions, squeezing their textured surface(s) into the film. Roll-to-roll processes can be implemented in many different forms. The thermal form of NIL can be used to emboss nanoscale topology on the film or substrate by using heated rollers. Likewise, there are examples of UV NIL being implemented to create textured surfaces with roll-to-roll devices. The traditional forms of gravure or flexography can also be adapted to create roll-to-roll NIL transfer printing processes.

19.5.2 Fundamental Issues

There are a few commercial products being made with imprint today, proof that the technology is inherently manufacturable. Some of the companies operating in this space include Nano Opto, Heptagon, Omron, OVD Kingram, LG Electronics, Reflexite, MacDermid, Wavefront Technologies, and Spectratek.

Dr. Michael P.C. Watts is the founder and president of Impattern Solutions, an independent consulting company in the field of NIL. The company's website tracks the progress and commercialization of imprint-related technologies and provides updates at www.impattern.com. Most of the commercial success stories in the imprint field have thus far been related to optics or light. These include, in order of decreasing critical dimensions, refractive, diffractive, and sub-wavelength optical devices. However, even with the sub-wavelength devices, the minimum dimensions of the structures being fabricated commercially are typically on the order of 100 nm or larger, which by many definitions, is not within the nanoscale domain. The community has yet to see the realization of devices fabricated by NIL with dimensions strongly into the sub-100 nm regime. There are many examples of nanoelectronic technologies in the R&D phase that appear to have strong potential with respect to NIL, but several fundamental issues need to be resolved before these ideas can successfully make the transition from the lab to manufacturing. In this section, we briefly summarize some of the remaining technical roadblocks to the commercialization of nanoelectronics via NIL techniques.

19.5.2.1 Nanoimprint Materials Development

There are several examples of high resolution patterning being achieved with NIL. For years, Professor Chou's fabrication of 10 nm vias was the ultimate demonstration of high resolution patterning with NIL.¹⁶⁸ More recently, Professor John Roger's group demonstrated that the fabrication of 2 nm replicas of carbon nanotubes randomly distributed across a rigid substrate could be created within a polydimethylsiloxane (PDMS) resin using NIL processes.¹⁸⁰ Professor Chou's group has gone on to report the patterning periodic line-space patterns with a 6 nm half-pitch,¹⁸¹ indicating that NIL has the potential resolution and patterning control that is commensurate with nanoelectronics (Figure 19.15).

However, there is still a need for improving NIL materials or resists. Resolution is only part of the picture and a NIL resist must also satisfy a number of different properties. First, the material must be able to readily flow into the imprint mold. If harsh conditions that plastically deform the patterned material are required, the NIL processes may induce residual stress into the patterns.¹⁸²⁻¹⁸⁴ It is desirable that the patterned media readily flows into the imprint mold. Likewise, the imprinted patterns must have the mechanical strength to resist pattern collapse. There are several examples of the critical aspect ratio for pattern collapse with decreasing feature size.¹⁸⁵ NIL is capable of generating very small patterns that make pattern collapse a significant concern. Furthermore, it is critical that the mold separates easily from the imprinted structure without destroying the sample. This requires both low surface energy mold treatment strategies that minimize adhesion between the imprint and the substrate as well as imprint materials with the cohesive strength to withstand the shear stress generated during mold separation.¹⁸⁶ Since external forces are required to pry the mold from the substrate, a mechanical load is placed on the

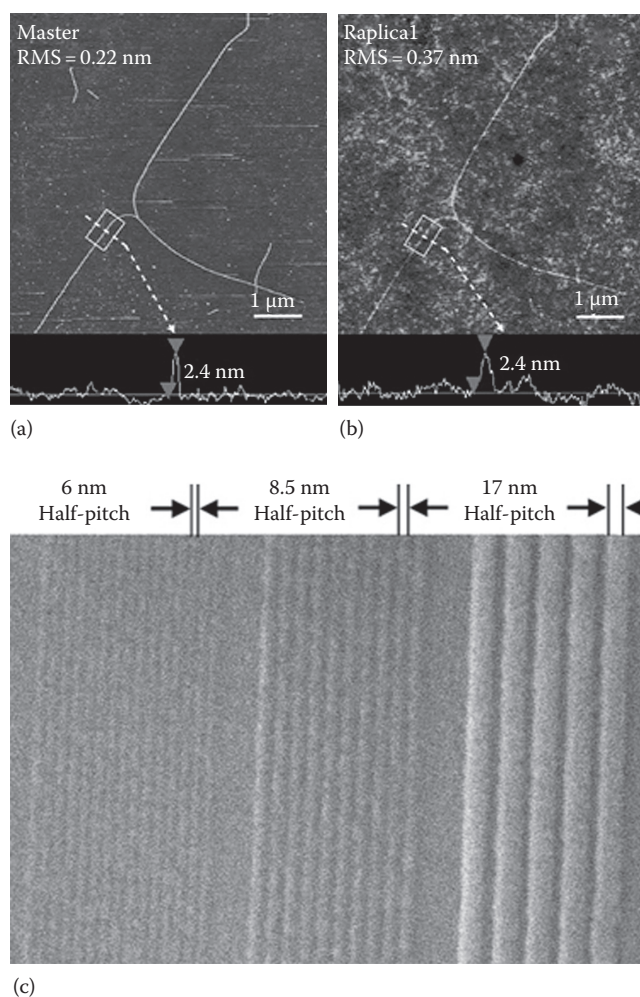


FIGURE 19.15 Examples of high resolution patterning with NIL. Panels (a) shows a few carbon nanotubes with a diameter of 2 nm on a flat surface that served as the model imprint mold while panel (b) shows the resulting patterns that were replicated in PDMS. (Reprinted from Hua, F. et al., *Nano Lett.*, 4(12), 2467, 2004. With permission.) Panel (c) shows well regular line-space patterns that have been imprinted with critical dimension to a 6 nm half-pitch. (Reprinted from Austin, M.D. et al., *Nanotechnology*, 16(8), 1058, 2005. With permission.)

patterns. It is a significant materials science challenge to maximize these properties simultaneously especially with functional nanoimprint materials.

19.5.2.2 Template Fabrication and Availability

The fabrication and availability of high quality templates or molds are crucial for NIL patterning technologies. With an ultimate resolution approaching just a few nm, even the slightest flaw in the master has the potential to be replicated into hundreds or thousands of imprinted copies. This means that significant efforts must be made to produce high quality imprint masters. Electron-beam (e-beam) lithography is the industry standard for producing high-resolution patterns with a resolution on the order of 10–20 nm. However, e-beam

lithography is not practical for manufacturing since it is a slow, serial writing process and is very costly. One of the greatest attributes of NIL is that it can be considered as an e-beam replication technique. Once a costly pattern is fabricated by e-beam lithography into a mold or master material, thousands of high-resolution copies of the pattern can be replicated via NIL processes at a fraction of the initial cost.¹⁸⁷ This is a very attractive proposition, but it also means that a high quality imprint master is critical. Any mistake will be easily propagated through all of the copies.

19.5.2.3 Defect Inspection and Dimensional Metrology

The need to have high quality imprint templates has been articulated in the preceding section. Hand-in-hand with this requirement is the need to evaluate, quantify, and certify the pattern quality in both the imprint master and the resulting imprints. High-resolution patterning demands high-resolution pattern metrology. We have already mentioned the excessive costs for fabricating a NIL master or mold with large areas patterned with nanoscale features. Quantitative measurements to qualify that the imprint master meets the design specifications in terms of pattern shape are absolutely critical for making this investment. Likewise, fast and efficient high-resolution pattern metrology methods are also needed to monitor the high volume manufacturing processes. It is critical to have quantitative measures in place to determine if the manufacturing processes drift out of tolerance. For high-resolution patterning, this means high-resolution metrology. Even at the current 65 nm technology node, the “Metrology” chapter of the ITRS Roadmap contains roadblocks in terms of high-resolution CD metrologies.¹⁸⁸ The leap from 65 nm optical lithography to NIL processes that offer better than a 5 nm resolution raise significant concerns regarding our ability to quantitatively evaluate the patterns that we fabricate. This is not that big of an issue in the R&D phase of technology development, where one usually deals with highly optimized prototypes. However, high volume manufacturing processes demand quantitative process monitoring capabilities. With respect to pattern shape metrology, the ability to pattern with NIL greatly exceeds the limits of the current inspection tools.

NIL is essentially a direct pattern transfer process whereby the patterns in the imprint have the potential to be a mirror image of the patterns in the mold. This brings up the fidelity of the pattern transfer concept—how closely do the imprinted features resemble the mold. To achieve the greatest fidelity of pattern transfer, one must be able to minimize the shrinkage of the imprinted material in the mold (either up cross-linking or cooling) or any distortions of the pattern after imprinting. The fidelity of the pattern transfer concept is fundamentally unique to NIL. However, in NIL one can directly compare the dimensions of the mold cavity to the pattern to quantify the fidelity of the pattern transfer. This means that dimensional metrologies must be able to quantify both the mold and the imprinted patterns.¹⁸⁹

19.5.2.4 Residual Layer Control

The objective in most imprint processes is typically to create isolated patterns on the substrate. However, there is always a continuous residual layer of resist material between the substrate and the patterns that needs to be removed. Simple volume filling arguments dictate the thickness of the residual layer, comparing the volume of material per unit area in the smooth film to the volume of the cavities in the mold. Even if there is less material in the film than there is in the mold cavities, the protrusions of the mold cannot be completely pressed into direct contact with the substrate; there is always a finite residual layer on the order of a few nanometers thick. While this residual layer is easily removed through reactive ion etching (RIE) processes, it is critical to achieve both a minimized and uniform residual layer. The minimized residual layer is important to maintain CD control. RIE processes are highly anisotropic, etching primarily vertically, however, there is a small amount of lateral trimming that occurs (Figure 19.16). If one has to etch through a thick residual layer, then the extent of lateral trimming can be significant; minimizing the residual layer minimizes the trimming. Furthermore, it is important to achieve a uniform residual layer across the entire field of the imprint. If there are thick and thin regions of residual layer, the RIE will break through to the substrate first in the thinner regions. When this happens, a micro loading effect occurs in the etch process where the concentration of plasma increases upon breakthrough (the plasma etch chemistries are biased to consume resist over the substrate). The result of micro-loading is an increased lateral etch rate, i.e., a localized enhancement in the lateral trimming. This nonuniform lateral trimming leads to a distribution of the pattern dimensions (loss of CD control).

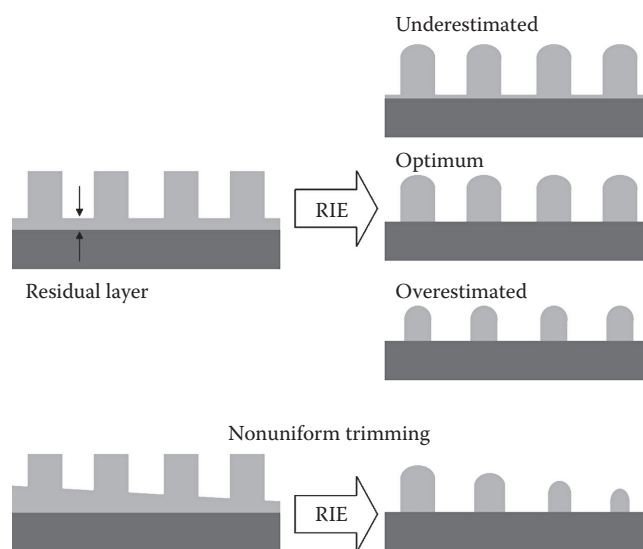


FIGURE 19.16 A schematic illustrating how an accurate knowledge and control of the residual layer thickness is critical to controlling lateral trimming and critical dimension control. Overestimating the thickness of the residual layer can lead to excessive lateral trimming. A non-uniform residual layer can lead to a distribution of linewidths and a loss of CD control through a micro-loading effect.

Controlling the residual layer thickness is straight forward for imprint molds with uniform pattern fields. Simple volume filling calculations can be used to adjust the thickness of the film to minimize the residual layer, assuming that a uniform pressure is applied.¹⁹⁰ However, residual layer control becomes difficult when the pattern field contains a distribution of different patterns with different sizes and density. In this case, the volume filling calculations are different for the different regions of the mold.¹⁹¹ Resist films are usually applied via spin coating techniques, which leads to a film of uniform thickness. In these situations, it is difficult to control the residual layer. The Molecular Imprints series of tools use a GDS-based drop on demand technology to deposit an optimized amount of resist material in each location to properly fill the mold. This technique can be very effective for minimizing the residual layer.^{192,193}

19.5.3 Overlay Accuracy and Control

Depending on the application, it may or may not be important to align the imprint within the lateral directions with some features or fiducial markers on the substrate. There are many applications, such as anti-reflective optical coatings, where pattern overlay is not required. However, for nanoelectronic applications, one could imagine it being very important to align the imprint with circuit elements in the substrate. Most imprint tools offer some type of alignment capability. The alignment is usually achieved by fabricating a series of vernier gratings in both the imprint mold and the patterning substrate and use interferometers to sense very small changes in the in-plane dimensions.¹⁹⁴ Piezoelectric actuators can be incorporated into the imprint head to generate very small lateral position corrections that help precisely align the mold with the substrate. Most general use imprint tools are designed for molds and substrates that are not transparent, meaning that the comparison of the interference pattern from the two verniers is achieved through a series of mirrors and reflective light. With these types of tools, one is able to achieve overlay accuracies on the order of ± 200 nm in the in-plane directions. Given the 5 nm or better patterning resolution of NIL, the accuracy with which a feature can be placed within the plane of the film is significantly worse. There are tools with higher overlay accuracy. Molecular Imprints produces highly specialized tools that are optimized for patterning with UV radiation only, using quartz molds that are optically transparent.¹⁹⁵ When it comes to overlay alignment, systems that are dedicated to patterning with transparent molds have a significant advantage because through wafer comparison of the optical verniers is possible. Eliminating the series of mirrors and reflective optics reduces the error in the overlay alignment, enabling sub-15 nm 3σ overlay accuracy. This is more commensurate with the ultimate patterning resolution of a few nm.

19.5.4 Technology Examples

There are a growing number of examples in the literature of nanoelectronic devices being fabricated by NIL processes, proving that the technique has potential (Figure 19.17). The most

common examples are the cross-bar memory structures where a semiconducting material is sandwiched between orthogonally situated parallel line-space electrodes to be used as either data storage or logic devices.¹⁹⁶ Here, NIL processes are used to fabricate the parallel line-space electrode arrays. These devices can have half-pitch values as small as 17 nm for the electrode arrays and memory densities as high as 100 Gbit/cm². On the CMOS front, a recent joint effort from Toshiba and Molecular Imprints have demonstrated the fabrication of a functional sub-32 nm logic circuit using NIL.¹⁹⁷ Likewise, IBM and SEMATECH have reported the fabrication of 27 nm functional FINFET structures using NIL technologies.¹⁹⁸ Another sector where NIL processes are being widely adapted is for magnetic data storage media. The equivalent Moore's law for the hard disc industry is even more aggressive than that of the semiconductor industry, doubling in data storage capacity ever 12 months. To keep pace with this trend, the industry is moving towards bit patterned media. NIL processes are being developed to fabricate 25 nm posts of magnetic media on a pitch of approximately 40 nm.¹⁹⁹ These are just a few examples related to nanoelectronics where NIL technologies are being actively pursued. There are also a number of other applications in the optical and biotechnology fields where NIL methods are poised to have an impact. Two of the most prominent examples include wire grid polarizer elements for screen and display technologies^{200,201} and photonic structures to facilitate light extraction in high brightness LEDs.¹⁸⁷

19.5.5 Future Perspectives

In some respects, NIL is just one of a long list of next-generation lithography techniques that has been developed as an alternative to deep UV optical lithography for the semiconductor industry. However, none of these alternate technologies have even come close to supplanting optical lithography as the high volume lithography of choice for the electronics industry. While a debate over the merits of NIL to replace optical lithography for CMOS fabrication is beyond the scope of this review, it is important to realize that NIL is the first next generation lithography candidate to have a viable life outside of CMOS, and there are already success stories for the patterning technology in non-CMOS technologies. This means that the success or failure of NIL is not tied to the semiconductor industry; it has already succeeded. As microelectronics moves beyond CMOS into nanoelectronics with novel device architectures, dramatically different principals of operation, and the need for nanoscale patterning, NIL is on-pace to be a well-established generic nanoscale patterning technology of relevance. Next generation lithography techniques tied directly to the CMOS community (193 nm immersion, double patterning, EUV) are solely dependent on this community for success or failure. These patterning technologies will likely go away if they are not adapted by the semiconductor community. The same is not true for NIL.

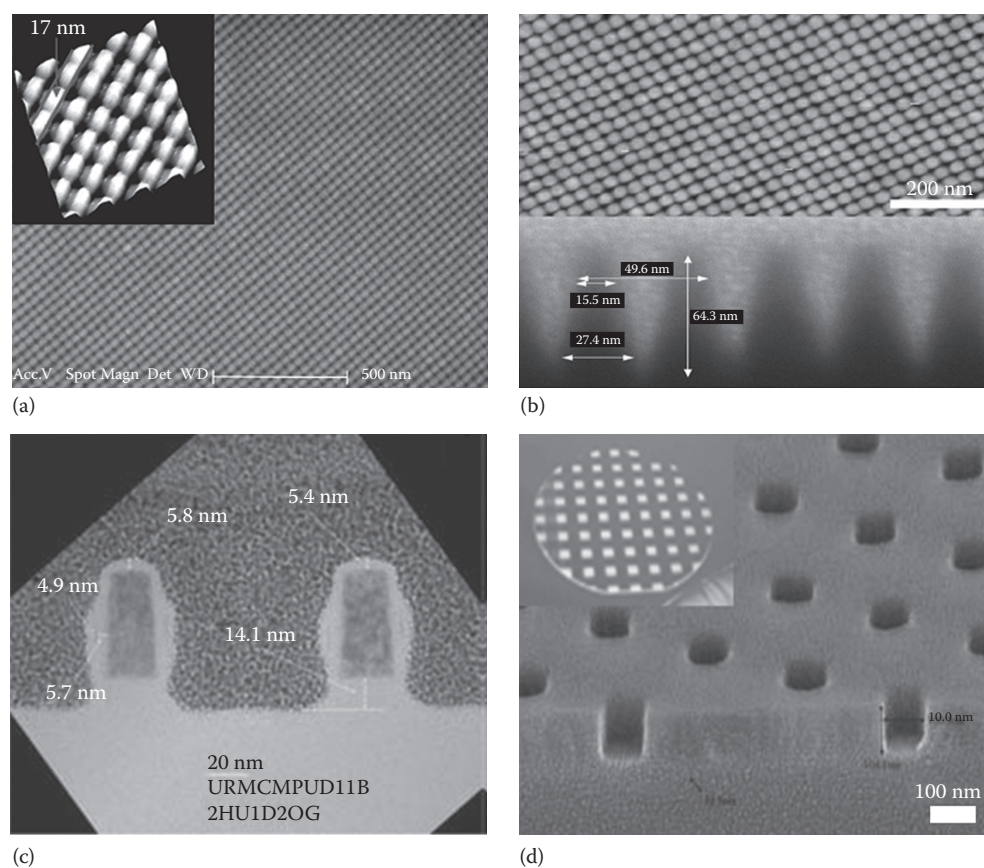


FIGURE 19.17 Examples of several different technologies fabricated with NIL techniques: (a) a high-resolution image taken from the 17 nm half-pitch cross-bar nanowire circuit arrays made by SNAP. (Reprinted from Jung, G.Y. et al., *Nano Lett.*, 6(3), 351, 2006. With permission.) (b) Bit patterned magnetic media for high density data storage showing 25 nm magnetic posts fabricated by NIL. (Reprinted from Dobisz, E.A. et al., *Proc. IEEE*, 96(11), 1836, 2008. With permission.) (c) A cross-sectional view of a functional 27 nm FinFET structure whose critical dimension was patterned by Step-and-Flash Imprint Lithography at Molecular Imprints. Nominally identical structures led to functional FinFET devices. Permission to reproduce this image was granted by the IBM Almaden Research Center, San Jose, CA. (d) An array of photonic devices patterned uniformly over an entire 6 nm wafer for high brightness LED devices. (Reprinted from Miller, M. et al., *Proc. SPIE*, 6883, 68830D, 2008. With permission.)

19.6 Metrology for Nanolithography

19.6.1 Advanced Lithographic Processes

As optical lithography reaches its limits, new processes such as double patterning and double exposure are being explored as means of extending 193 nm immersion-based lithography. The goal of these patterning methods is patterning at dimensions that are less than those that can be printed in a single lithographic exposure step. Each of these process-based methods poses a unique challenge to all aspects of process control including metrology. These processes are summarized in Figures 19.18 through 19.20.¹⁸⁸

Double exposure uses two reticles that must be precisely aligned so that the pattern placement is one pitch across the printed area. One photoresist layer is exposed twice with specially designed reticles resulting in densely spaced lines. This pattern can then be etched into the underlying films patterning the wafer with features having a $\frac{1}{2}$ pitch less than can be printed using one reticle. This process is shown in Figure 19.18.

Double patterning is also done using two reticles that must be aligned with accuracy, so that the pattern placement has one pitch and close to one linewidth across the printed area. The first photoresist layer is exposed and then the film stack is etched leaving the pattern in the hard mask layer. Then the wafer is coated with BARC and resist and the second set of lines is patterned into the second BARC/resist layer. The resultant double pattern structure is etched into the poly silicon. Figure 19.19 provides great detail for double patterning processes for lines. Similar process steps are used for contacts and trenches.

Spacer double patterning is believed to be already in use in manufacturing. A slightly different film stack is used for spacer double patterning. First, a sacrificial poly silicon layer is patterned, spacer oxide is deposited, and the sacrificial poly silicon layer is removed resulting in a spacer pattern. This pattern is etched into the poly silicon layer. In Figure 19.20, this single reticle process is more fully described. The origin of the two sets of line shapes is due to the different shapes of each side of a spacer. The two sets of critical dimensions are due to the nature of the spacer deposition process.

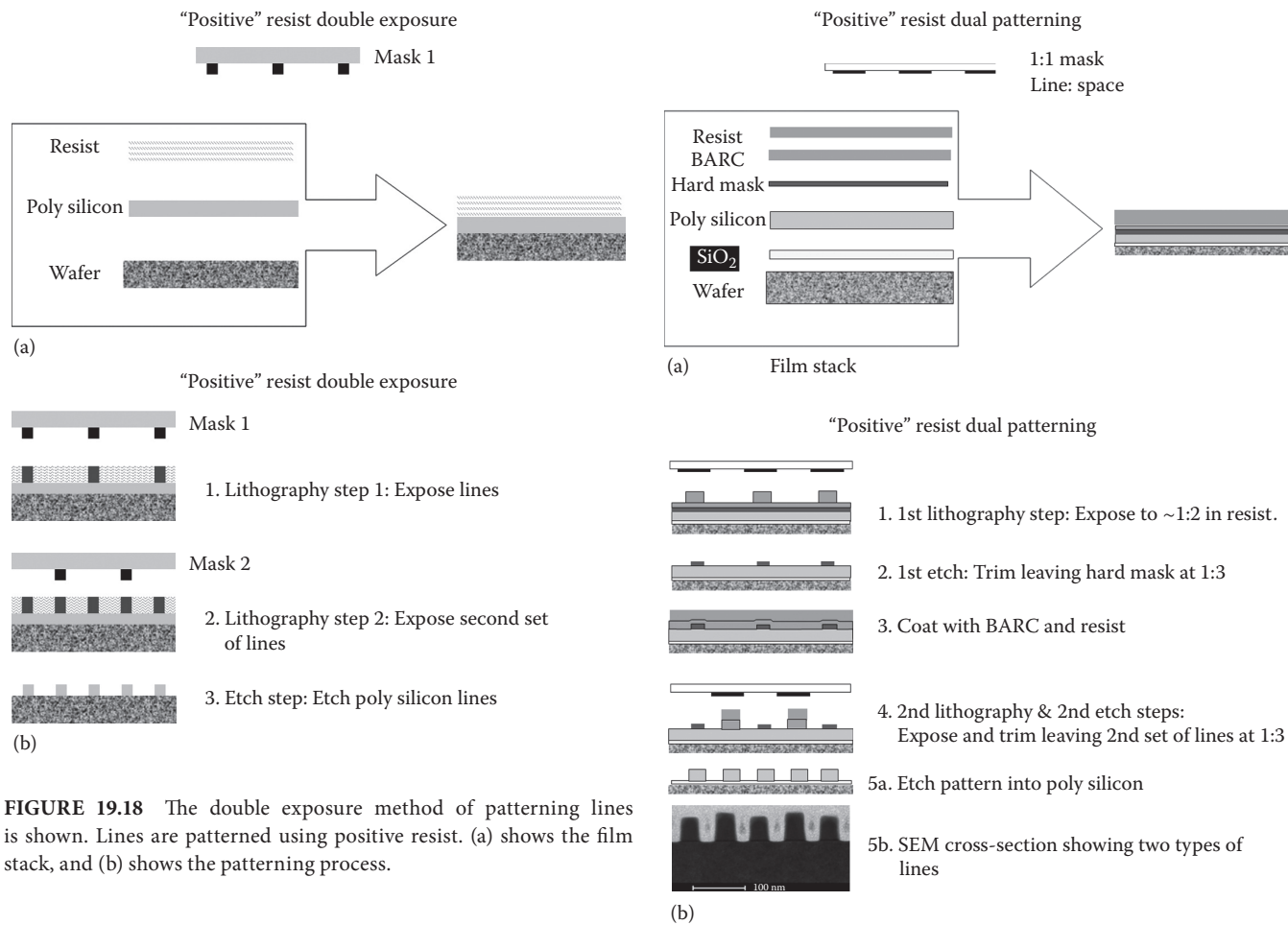


FIGURE 19.18 The double exposure method of patterning lines is shown. Lines are patterned using positive resist. (a) shows the film stack, and (b) shows the patterning process.

FIGURE 19.19 The double patterning method of patterning lines is shown. Lines are patterned using positive resist. (a) shows the film stack, and (b) shows the patterning process.

Overlay plays an important role in double patterning, spacer patterning, and double exposure patterning of lines. Overlay must be near perfect to achieve a uniform pitch. If the second exposure is shifted, every other space will be different. This impacts further processing, the measurement of CD and lineshape, and device performance. Etch is known to be sensitive to lineshape and the distance between lines. Etch uniformity can be reduced when the resist pattern is etched into the layer below.

19.6.2 Metrology for Advanced Lithography Processes

Measurement needs start with control of feature shape and placement on the mask (reticle), and follow through until the features are etched into the active layer of the device or interconnect structure.¹⁸⁸ Since optical masks are glass with chrome features, scanning electron microscope (SEM)-based measurements must overcome the charging inherent in the measurement of an insulator. The chrome features must have the correct linewidth and shape and must be placed on the mask in the correct position relative to each other. The recent introduction of "environmental" SEM allows for charge neutralization during the SEM-based measurement of CD and line shape on the mask.

The advanced lithographic process challenge metrology mainly through the two distributions of critical dimensions

and line shapes especially the side wall angles of the lines. Two methods of CD measurement are used during manufacturing, namely CD-scanning electron microscopy (CD-SEM) and scatterometry. The term scatterometry typically refers to one of two optical methods of measuring critical dimensions using a grating test structure. One example of a grating test structure is an array of lines with a constant pitch and linewidth. Others include an array of contact holes. Scatterometry measurements can be done in a spectroscopic ellipsometer; the main challenge is analyzing the changes in the optical response that the grating structure imparts versus the response of an un-patterned film stack. The other approach to scatterometry is to measure the diffraction pattern from a single wavelength across a range of angles. Both methods of scatterometry require that an extensive database of simulated ellipsometric responses be placed into a library. Some libraries contain tens to hundreds of thousands of simulated structures for a single process step. Data from a sample is matched to this set of simulated responses. Accuracy requires that ellipsometry be sensitive to the small differences in optical response.

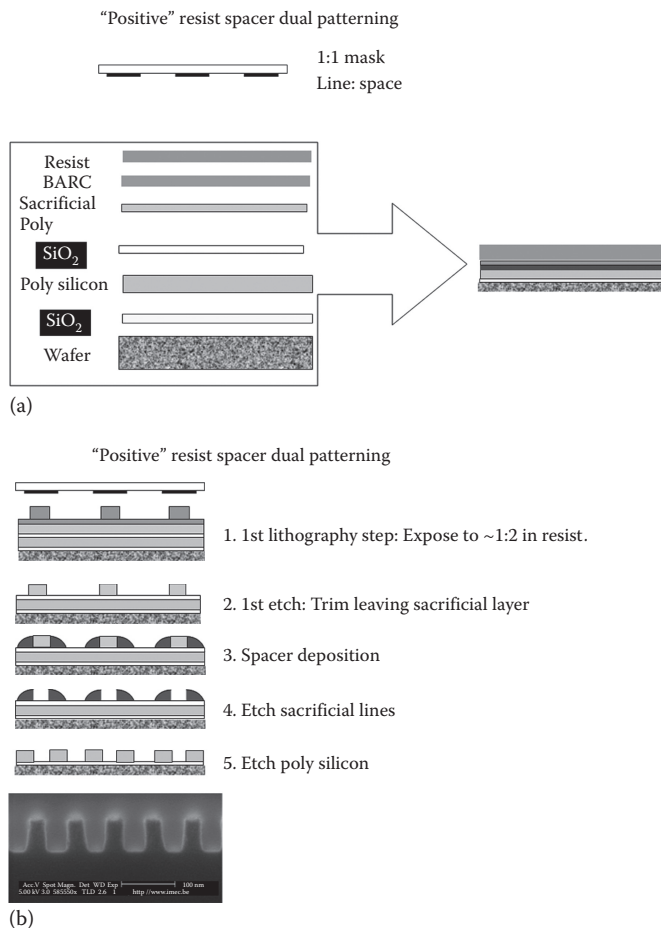


FIGURE 19.20 The spacer double patterning method is shown. Lines are patterned using positive resist. (a) shows the film stack, and (b) shows the patterning process.

Ellipsometry measures the change in polarization of light after reflection from the sample surface. Spectroscopic ellipsometry-based scatterometry relies on the changes in polarization due to changes in the grating test structure as a function of wavelength. Advanced lithographic processes pose two challenges to scatterometry. One is shrinking feature size and the second is the two sets of distributions of CD and feature shape. Sensitivity to small changes in dimension is becoming increasingly difficult as feature size decreases below 50 nm for both CD-SEM and scatterometry. The previous method of single exposure and etch patterning required that scatterometry measure the average CD and line shape of a uniform grating structure. Double patterning and double exposure requires that scatterometry produce the average CD and line shape of two distributions of line shape. In situations where overlay errors result in a nonuniform pitch, the number of simulated data sets is greatly increased. Small differences in optical response make it very difficult to distinguish changes in CD and line shape. Recent commercial instrumentation extended the wavelength range of scatterometry further into the UV down to 150 nm. In general, UV wavelengths have

improved the ability of scatterometry to measure CD and line shape for features with sub 50 nm dimensions.

The specifics of ellipsometry-based scatterometry are useful in understanding how critical dimensions are determined from a method associated with the determination of film thickness for unpatterned layers. The premise of ellipsometry is that light polarized in-plane of reflection (P) reflects differently than light polarized perpendicular to the plane of reflection (S). Ellipsometry determines the change in polarization of light in terms of Δ , which is the difference in phase change $= \Delta_p - \Delta_s$ and Ψ , which is related to the ratio of the change in intensity upon reflection through $\tan^{-1} (|R_p|/|R_s|)$, where R_p and R_s are the complex reflectivity's parallel and perpendicular to the reflectance plane. The reflectivity is determined by the dielectric function of the film stack. Reflection from a single film on a substrate depends on the complex dielectric function (refractive index) of the materials and the Fresnel reflection coefficients r_{12} between (1) air and (2) the film and r_{23} between (2) film and (3) the substrate. The reflection from an unpatterned film is determined by well-understood reflection coefficients²⁰²

$$R_p = \frac{(r_{12}^p + r_{23}^p e^{-i2\beta})}{(1 + r_{12}^p r_{23}^p e^{-i2\beta})} \quad (19.6)$$

$$R_s = \frac{(r_{12}^s + r_{23}^s e^{-i2\beta})}{(1 + r_{12}^s r_{23}^s e^{-i2\beta})} \quad (19.7)$$

where

$$\beta = 2\pi \left(\frac{d}{\lambda} \right) N_2 \cos \phi \quad (19.8)$$

The film thickness dependence comes from the exponential term β where d is the film thickness, λ is the wavelength of the light, and N_2 is the complex refractive index of the film. The measurement of a patterned film stack requires that Maxwell's equations be solved. Typically, this is done using a rigorous coupled wave approximation (RCWA), and the RCWA equations must be solved at each wavelength for each structure. Changes in Ψ and Δ vs wavelength require solving the RCWA equations at enough wavelengths to observe subtle changes due to CD and line shape.²⁰²

The CD-SEM measurement of critical dimensions is also challenged by double patterning and double exposure. Measuring patterned photoresist requires the calibration of the rate of shrinkage of the resist vs. electron beam exposure time. This calibration requires the collection of enough data to provide statistically significant shrinkage rates. This must be done for each resist material. It is important to note that different resists are used for the fabrication of line and vias. Many IC manufacturers hold the resist formulas to be proprietary meaning that each

resist formula will have different responses to electron beam exposure. Recent unpublished studies show that resist lines with a CD less than 25 nm shrink more rapidly than lines with a greater CD. Scatterometry measurements may also impact resist lines especially when measurements are done in UV.

There are important differences between CD-SEM and scatterometry in terms of the nature of information each provides. Advanced CD-SEM is capable of measuring the CD of two or more lines simultaneously. Future CD-SEMs may be able to measure several lines in a test area providing the average CD as well as the range of the CD in the test area. Scatterometry provides the average CD in the test area.

The measurement of line edge roughness in resist is critical for the control of device performance including leakage current. Industry standards organizations such as SEMI have driven consensus documents describing measurement methods for quantifying line edge roughness.²⁰³ Line edge roughness on a nm scale produces gate CD width roughness that results in an increase in leakage current. Line edge roughness at longer scales produces an increase in carrier surface scattering that increases line resistivity. At this time, line edge roughness measurements can be done using CD-SEM or CD-AFM.

Overlay metrology is considerably more challenging for advanced lithography processes. Overlay measurements are typically done using specially designed optical microscopes and target structures that are patterned into both the upper and lower layers. Double patterning of trenches for interconnect lines have additional complications for metrology. If the overlay is shifted, then the trench CD also changes. Overlay measurement precision for all double patterning methods becomes at best a factor of 0.7 of the overlay required for a single exposure patterning of all the trenches. This has driven the development of new overlay test structures that include scattering bars that diffract light. SEM may provide an alternate means of measuring overlay.

19.6.3 Proposed New CD Metrology Methods

Many have speculated about the demise of CD-SEM and scatterometry. Even optical microscopy-based CD measurement is still done for features have larger CDs such as microelectromechanical systems (MEMS). It is possible that CD-SEM and scatterometry can not extend beyond the 22 nm half pitch. Two methods are being considered as potential replacements for scatterometry and CD-SEM. These are small angle x-ray scattering, which is known as CD-SAXS,²⁰⁴ and He ion microscopy.²⁰⁵ In CD-SAXS, a focused, monochromatic x-ray beam is transmitted through a grating test structure, as shown in Figure 19.21, that is similar to the ones used for scatterometry measurement. It is important to note that CD-SAXS can measure line edge roughness, average CD, individual CD, and line shape for the lines in the test structure.²⁰⁶⁻²⁰⁹ At this time (2009), evaluation of the capabilities of He ion microscopy are in the initial stages.

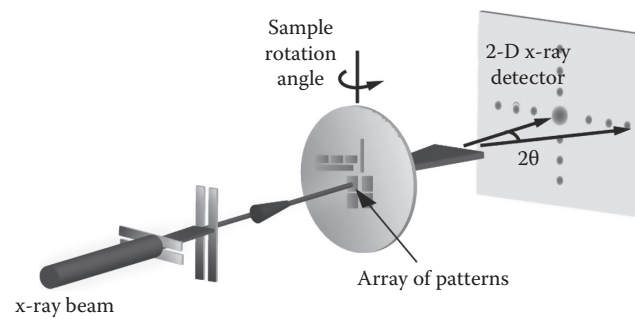


FIGURE 19.21 CD SAXS schematic of using collimated x-ray beams with energy that are transmissive through a patterned silicon wafer resulting in scattering from an array of patterns.

Abbreviations

α	Fraction of light absorbed, when referring to resist technology
α	Width of the forward-scattering distribution, when referring to electron-beam lithography
β	Width of the backscattered distribution, when referring to electron-beam lithography
δ	Photoacid diffusion length, when referring to resist technology
ϵ	Photoacid generation efficiency, when referring to resist technology
η	The effective dose contributed by the backscattered electrons, when referring to electron-beam lithography
BARC	Bottom anti-reflective coating
CD	Critical dimension
CD-SEM	Critical dimension scanning electron microscope
CD-SAXS	Critical dimension small-angle x-ray scattering
CD-AFM	Critical dimension atomic force microscopy
CMOS	Complementary metal-oxide semiconductor
CMP	Chemical mechanical polishing
De	Dose at line-edge, when referring to resist technology
D_0	Incident dose, when referring to electron-beam lithography
DOF	Depth of focus
DUV	Deep-ultraviolet
E_0	Incident electron energy, when referring to electron-beam lithography
EUV	Extreme-ultraviolet
FINFET	Nonplanar, double-gate field effect transistor, “fin” refers to shape of semiconductor
HP	Half-pitch
HSQ	Hydrogen silsesquioxane
IC	Integrated circuit
ITRS	<i>International Technology Roadmap for Semiconductors</i>
LILS	Latent-image log slope
LED	Light emitting diode

LER	Line-edge roughness
LWR	Line-width roughness
MEMS	Microelectromechanical systems
MG	Molecular glass
ML2	Maskless lithography
NA	Numerical aperture
NIL	Nanoimprint lithography
PAG	Photoacid generator
PDMS	Polydimethylsiloxane
q	Number of photons/nm ² , when referring to resist technology
RIE	Reactive ion etch
SCALPEL	Scattering with angular limitation in projection electron-beam lithography
STM	Scanning tunneling microscopy
UV	Ultraviolet

References

- Moore, G. E., Cramming more components onto integrated circuits, *Electronics*, **38**, 114–117 (1965).
- Huff, H., *Into the Nano Era*, Springer Series in Materials Science, Springer-Verlag, Berlin, Germany, **106**, (2009).
- Maydan, D., Coquin, G. A., Maldonado, J. R. et al., High-speed replication of submicron features on large areas by x-ray lithography, *IEEE Transactions on Electron Devices*, **ED22**(7), 429 (1975).
- Silverman, J. P., X-ray lithography: Status, challenges, and outlook for 0.13 μm , *Journal of Vacuum Science & Technology B*, **15**(6), 2117 (1997).
- Harriott, L. R., Berger, S. D., Biddick, C. et al., The SCALPEL proof of concept system, *Microelectronic Engineering*, **35**(1–4), 477 (1997).
- Liddle, J. A., Berger, S. D., Biddick, C. J. et al., The scattering with angular limitation in projection electron-beam lithography (SCALPEL) system, *Japanese Journal of Applied Physics Part 1—Regular Papers Short Notes & Review Papers*, **34**(12B), 6663 (1995).
- Tennant, D., Limits of conventional lithography, in G. M. Timp (ed.), *Nanotechnology*, AIP/Springer, New York, Chap. 4, p. 161 (1999).
- Marrian, C. R. K. and Tennant, D. M., Nanofabrication, *Journal of Vacuum Science & Technology A*, **21**(5), S207–S215 (2003).
- Brunner, T. A., Why optical lithography will live forever, *Journal of Vacuum Science & Technology B*, **21**(6), 2632 (2003).
- Levinson, H. J., *Principles of Lithography*, 2nd edn., SPIE Press, Bellingham, WA, (2005).
- Brillouet, M., An introduction to ultimate lithography, *Comptes Rendus Physique*, **7**(8), 837 (2006).
- Ito, H., Chemical amplification resists for microlithography, *Advances in Polymer Science*, **172**, 37 (2005).
- Chandhok, M., Datta, S., Lionberger, D., and Vesecky, S., Impact of line-width roughness on Intel's 65-nm process devices, *Advances in Resist Materials and Processing Technology XXIV, SPIE*, **6519**, 65191A (2007).
- International Technology Roadmap for Semiconductors*, 2007 edition, <http://www.itrs.net>, Lithography, p. 10. SEMATECH, Austin, TX.
- Wallraff, G. M. and Hinsberg, W. D., Lithographic imaging techniques for the formation of nanoscopic features, *Chemical Reviews*, **99**(7), 1801 (1999).
- Gallatin, G. M., Naulleau, P., Niakoula, D. et al., Resolution, LER, and sensitivity limitations of photoresists, *Emerging Lithographic Technologies XII, SPIE*, **6921**, 69211E (2008).
- Bristol, R. L., The tri-lateral challenge of resolution, photo-speed, and LER: Scaling below 50 nm? *Advances in Resist Materials and Processing Technology XXIV, SPIE*, **6519**, 65190W (2007).
- Van Steenwinckel, D., Gronheid, R., Lammers, J. H. et al., A novel method for characterizing resist performance, *Advances in Resist Materials and Processing Technology XXIV, SPIE*, **6519**, 65190V (2007).
- Wallow, T., Higgins, C., Brainard, R. et al., Evaluation of EUV resist materials for use at the 32 nm half-pitch node, *Emerging Lithographic Technologies XII, SPIE*, **6921**, 69211F (2008).
- Fedyunshyn, T. H., Goodman, R. B., and Roberts, J., Polymer matrix effects on acid generation, *Advances in Resist Materials and Processing Technology XXV, SPIE*, **6923**, 692319 (2008).
- Pawloski, A. R., Christian, and Nealey, P. F., A standard addition technique to quantify photoacid generation in chemically amplified photoresist, *Chemistry of Materials*, **13**(11), 4154 (2001).
- Szmanda, C. R., Brainard, R. L., Mackevich, J. F. et al., Measuring acid generation efficiency in chemically amplified resists with all three beams, *Journal of Vacuum Science & Technology B*, **17**(6), 3356 (1999).
- Brainard, R., Hassanein, E., Li, J. et al., Photons, electrons, and acid yields in EUV photoresists: A progress report, *Advances in Resist Materials and Processing Technology XXV, SPIE*, **6923**, 692325 (2008).
- Hinsberg, W., Houle, F. A., Hoffnagle, J. et al., Deep-ultraviolet interferometric lithography as a tool for assessment of chemically amplified photoresist performance, *Journal of Vacuum Science & Technology B*, **16**(6), 3689 (1998).
- Pawloski, A., Acheta, A., Lalovic, I., LaFontaine, B., and Levinson, H., Characterization of line edge roughness in photoresist using an image fading technique, *Proceedings of the SPIE, Advances in Resist Technology and Processing XXI*, **5376**, 414 (2004).

AQ4

26. Houle, F. A., Hinsberg, W. D., Sanchez, M. I., and Hoffnagle, J. A., Influence of resist components on image blur in a patterned positive-tone chemically amplified photoresist, *Journal of Vacuum Science & Technology B*, **20**(3), 924 (2002).
27. Houle, F. A., Hinsberg, W. D., Morrison, M. et al., Determination of coupled acid catalysis-diffusion processes in a positive-tone chemically amplified photoresist, *Journal of Vacuum Science & Technology B*, **18**(4), 1874 (2000).
28. Croffie, E., Yuan, L., Cheng, M. S. et al., Modeling influence of structural changes in photoacid generators on 193 nm single layer resist imaging, *Journal of Vacuum Science & Technology B*, **18**(6), 3340 (2000).
29. Itani, T., Yoshino, H., Fujimoto, M., and Kasama, K., Photoacid bulkiness on dissolution kinetics in chemically amplified deep ultraviolet resists, *Journal of Vacuum Science & Technology B*, **13**(6), 3026 (1995).
30. Vogt, B. D., Kang, S., Prabhu, V. M. et al., Measurements of the reaction-diffusion front of model chemically amplified photoresists with varying photoacid size, *Macromolecules*, **39**(24), 8311 (2006).
31. Vogt, B. D., Kang, S., Prabhu, V. M. et al., The deprotection reaction front profile in model 193 nm methacrylate-based chemically amplified photoresists, *Advances in Resist Technology and Processing XXIII, Proceedings of SPIE*, **6153**, 615316 (2006).
32. Shi, X. L., Effect of Coulomb interaction and pKa on acid diffusion in chemically amplified resists, *Journal of Vacuum Science & Technology B*, **17**(2), 350 (1999).
33. Goldfarb, D. L., Angelopoulos, M., Lin, E. K. et al., Confinement effects on the spatial extent of the reaction front in ultrathin chemically amplified photoresists, *Journal of Vacuum Science & Technology B*, **19**(6), 2699 (2001).
34. Lin, E. K., Soles, C. L., Goldfarb, D. L. et al., Direct measurement of the reaction front in chemically amplified photoresists, *Science*, **297**(5580), 372 (2002).
35. Vogt, B. D., Kang, S., Prabhu, V. M. et al., Influence of base additives on the reaction diffusion front of model chemically amplified photoresists, *Journal of Vacuum Science & Technology B*, **25**, 175 (2006).
36. Wu, W. L., Prabhu, V. M., and Lin, E. K., Identifying materials limits of chemically amplified photoresists, *Advances in Resist Materials and Processing Technology XXIV, SPIE*, **6519**, 651902 (2007).
37. Lavery, K. A., Choi, K. W., Vogt, B. D. et al., Fundamentals of the reaction-diffusion process in model EUV photoresists, *Advances in Resist Technology and Processing XXIII, SPIE*, **6153**, 615313 (2006).
38. Houlihan, F., Person, D., Nalamasu, O. et al., Study of base additives for use in a single layer 193 nm resist based upon poly(norbornene/maleic anhydride/acrylic acid/tert-butyl acrylate), *Proceedings of the SPIE—The International Society for Optical Engineering*, **4345**, 67 (2001).
39. Pawloski, A. R., Christian, and Nealey, P. F., The multifunctional role of base quenchers in chemically amplified photoresists, *Chemistry of Materials*, **14**(10), 4192 (2002).
40. Houle, F. A., Hinsberg, W. D., and Sanchez, M. I., Acid-base reactions in a positive tone chemically amplified photoresist and their effect on imaging, *Journal of Vacuum Science & Technology B*, **22**(2), 747 (2004).
41. Hinsberg, W. D., Houle, F. A., Sanchez, M. I., and Wallraff, G. M., Chemical and physical aspects of the post-exposure baking process used for positive-tone chemically amplified resists, *IBM Journal of Research and Development*, **45**(5), 667 (2001).
42. Hinsberg, W., Houle, F., Sanchez, M. et al., Effect of resist components on image spreading during postexposure bake of chemically amplified resists, *Proceedings of the SPIE—The International Society for Optical Engineering*, **3999**, 148 (2000).
43. Michaelson, T. B., Pawloski, A. R., Acheta, A., Nishimura, Y., and Willson, C. G., The effects of chemical gradients and photoresist composition on lithographically generated line edge roughness, *Proceedings of SPIE*, **5753**, 368 (2005).
44. Hinsberg, W., Houle, F. A., Lee, S. W., Ito, H., and Kanazawa, K., Characterization of reactive dissolution and swelling of polymer films using a quartz crystal microbalance and visible and infrared reflectance spectroscopy, *Macromolecules*, **38**(5), 1882 (2005).
45. Hinsberg, W. D., Houle, F. A., Ito, H., Kanazawa, K., and Lee, S. W., Kinetics of reactive dissolution of lithographic polymers, *Proceedings of the 13th International Conference on Photopolymers, Advances in Imaging Materials and Processes, RETEC 2003*, 193 (2003).
46. Hinsberg, W. D., Houle, F. A., and Ito, H., Reactive dissolution of lithographic copolymers, *Proceedings of the SPIE, Advances in Resist Technology and Processing XXI*, **5376**, 352 (2004).
47. Houle, F. A., Hinsberg, W. D., and Sanchez, M. I., Kinetic model for positive tone resist dissolution and roughening, *Macromolecules*, **35**(22), 8591 (2002).
48. Prabhu, V. M., Vogt, B. D., Kang, S. et al., Direct measurement of the spatial extent of the in situ developed latent image by neutron reflectivity, *Journal of Vacuum Science & Technology B*, **25**(6), 2514 (2007).
49. Prabhu, V. M., Vogt, B. D., Kang, S. et al., Direct measurement of the in situ developed latent image: The residual swelling fraction, *Proceedings of SPIE*, **6519**, 651910 (2007).
50. Prabhu, V. M., Rao, A., Kang, S., Lin, E. K., and Satija, S. K., Manipulation of the asymmetric swelling fronts of photoresist polyelectrolyte gradient thin films, *The Journal of Physical Chemistry B*, **112**(49), 15628 (2008).
51. Wang, M. X., Gonsalves, K. E., Rabinovich, M., Yueh, W., and Roberts, J. M., Novel anionic photoacid generators (PAGs) and corresponding PAG bound polymers for sub-50 nm EUV lithography, *Journal of Materials Chemistry*, **17**(17), 1699 (2007).

52. Wang, M. X., Lee, C. T., Henderson, C. L. et al., Incorporation of ionic photoacid generator (PAG) and base quencher into the resist polymer main chain for sub-50 nm resolution patterning, *Journal of Materials Chemistry*, **18**(23), 2704 (2008).
53. Fukushima, Y., Watanabe, T., Ohnishi, R. et al., Optimization of photoacid generator in photoacid generation-bonded resist, *Japanese Journal of Applied Physics*, **47**(8), 6293 (2008).
54. Wu, H. P. and Gonsalves, K. E., Preparation of a photoacid generating monomer and its application in lithography, *Advanced Functional Materials*, **11**(4), 271 (2001).
55. Hirayama, T., Shiono, D., Hada, H., and Onodera, J., New photoresist based on amorphous low molecular weight polyphenols, *Journal of Photopolymer Science and Technology*, **17**(3), 435 (2004).
56. VanderHart, D. L., De Silva, A., Felix, N., Prabhu, V. M., and Ober, C. K., The effect of EUV molecular glass architecture on the bulk dispersion of a photo-acid generator, *Advances in Resist Materials and Processing Technology XXV, SPIE*, **6923**, 69231M (2008).
57. Young-Gil, K., Kim, J. B., Fujigaya, T., Shibasaki, Y., and Ueda, M., A positive-working alkaline developable photoresist based on partially tert-Boc-protected calix[4]resorcinarene and a photoacid generator, *Journal of Materials Chemistry*, **12**(1), 53 (2002).
58. Chang, S. W., Ayothi, R., Bratton, D. et al., Sub-50 nm feature sizes using positive tone molecular glass resists for EUV lithography, *Journal of Materials Chemistry*, **16**(15), 1470 (2006).
59. Yang, D., Chang, S. W., and Ober, C. K., Molecular glass photoresists for advanced lithography, *Journal of Materials Chemistry*, **16**(18), 1693 (2006).
60. De Silva, A., Lee, J. K., Andre, X. et al., Study of the structure-properties relationship of phenolic molecular glass resists for next generation photolithography, *Chemistry of Materials*, **20**(4), 1606 (2008).
61. Felix, N. M., De Silva, A., Luk, C. M. Y., and Ober, C. K., Dissolution phenomena of phenolic molecular glass photoresist films in supercritical CO₂, *Journal of Materials Chemistry*, **17**(43), 4598 (2007).
62. De Silva, A., Felix, N., Sha, J., Lee, J. K., and Ober, C. K., Molecular glass resists for next generation lithography, *Advances in Resist Materials and Processing Technology XXV, SPIE*, **6923**, 69231L (2008).
63. De Silva, A., Felix, N., Forman, D., Sha, J., and Ober, C. K., New architectures for high resolution patterning, *Advances in Resist Materials and Processing Technology XXV, SPIE*, **6923**, 69230O (2008).
64. Toriumi, M., Santillan, J., Itani, T., Kozawa, T., and Tagawa, S., Dissolution characteristics and reaction kinetics of molecular resists for extreme-ultraviolet lithography, *Journal of Vacuum Science & Technology B*, **25**(6), 2486 (2007).
65. Nishimura, I., Heath, W. H., Matsumoto, K. et al., Non-chemically amplified resists for 193 nm lithography, *Advances in Resist Materials and Processing Technology XXV, SPIE*, **6923**, 69231C (2008).
66. Lawson, R. A., Lee, C. T., Yueh, W., Tolbert, L., and Henderson, C. L., Single molecule chemically amplified resists based on ionic and non-ionic PAGs, *Advances in Resist Materials and Processing Technology XXV, SPIE*, **6923**, 69230K (2008).
67. Naulleau, P. P., Anderson, C. N., Chiu, J. et al., Latest results from the SEMATECH Berkeley extreme ultraviolet micro-field exposure tool, *Journal of Vacuum Science & Technology B* **27**,66-70(2009). AQ5
68. Woodward, J. T., Choi, K. W., Prabhu, V. M. et al., Characterization of the latent image to developed image in model EUV photoresists, *Advances in Resist Materials and Processing Technology XXV, SPIE*, **6923**, 69232B (2008).
69. Choi, K. W., Prabhu, V. M., Lavery, K. A. et al., Effect of photo-acid generator concentration and developer strength on the patterning capabilities of a model EUV photoresist, *Proceedings of SPIE*, **6519**, 651943 (2007).
70. Zimmerman, P. A., Byers, J., Piscani, E. et al., Development of an operational high refractive index resist for 193 nm immersion lithography, *Advances in Resist Materials and Processing Technology XXV, SPIE*, **6923**, 692306 (2008).
71. Matsumoto, K., Costner, E., Nishimura, I., Ueda, M., and Willson, C. G., High-index resist for 193-nm immersion lithography, *Advances in Resist Materials and Processing Technology XXV, SPIE*, **6923**, 692305 (2008).
72. Gonsalves, K. E., Wang, M., and Pujari, N. S., High refractive-index resists composed of anionic photoacid generator (PAG) bound polymers for 193 nm immersion lithography, *Advances in Resist Materials and Processing Technology XXV, SPIE*, **6923**, 69231P (2008).
73. Liu, H. P., Blakey, I., Conley, W. E. et al., Application of quantitative structure property relationship to the design of high refractive index 193i resist, *Journal of Micro-Nanolithography MEMS and MOEMS*, **7**(2), 023001 (2008).
74. Allen, R. D., Brock, P. J., Sundberg, L. et al., Design of protective topcoats for immersion lithography, *Journal of Photopolymer Science and Technology*, **18**(5), 615 (2005).
75. Terai, M., Kumada, T., Ishibashi, T. et al., Mechanism of immersion specific defects with high receding-angle topcoat, *Advances in Resist Materials and Processing Technology XXIV, SPIE*, **6519**, 65191S (2007).
76. Takebe, Y., Shirota, N., Sasaki, T., and Yokokoji, O., Development of top coat materials for ArF immersion lithography, *Advances in Resist Materials and Processing Technology XXIV, SPIE*, **6519**, 65191Y (2007).
77. Nakagawa, H., Goto, K., Shima, M. et al., Process optimization for developer soluble immersion topcoat material, *Advances in Resist Materials and Processing Technology XXIV, SPIE*, **6519**, 651923 (2007).

78. Sundberg, L. K., Sanders, D. P., Sooriyakumaran, R., Brock, P. J., and Allen, R. D., Contact angles and structure/surface property relationships of immersion materials, *Advances in Resist Materials and Processing Technology XXIV, SPIE*, **6519**, 65191Q (2007).
79. Shirota, N., Takebe, Y., Wang, S. Z., Sasaki, T., and Yokokoji, O., Development of non-topcoat resist polymers for 193-nm immersion lithography, *Advances in Resist Materials and Processing Technology XXIV, SPIE*, **6519**, 651905 (2007).
80. Wada, K., Kanna, S., and Kanda, H., Novel materials design for immersion lithography, *Advances in Resist Materials and Processing Technology XXIV, SPIE*, **6519**, 651908 (2007).
81. Wu, S., Tseng, A., Lin, B. et al., Non-topcoat resist design for immersion process at 32-nm node, *Advances in Resist Materials and Processing Technology XXV, SPIE*, **6923**, 692307 (2008).
82. Sanders, D. P., Sundberg, L. K., Brock, P. J. et al., Self-segregating materials for immersion lithography, *Advances in Resist Materials and Processing Technology XXV, SPIE*, **6923**, 692309 (2008).
83. Wang, D., Caporale, S., Andes, C. et al., Design consideration for immersion 193: Embedded barrier layer and pattern collapse margin, *Journal of Photopolymer Science and Technology*, **20**(5), 687 (2007).
84. Smith, B. W., Optics for photolithography, in K. Suzuki and B. W. Smith (eds.), *Microlithography: Science and Technology*, 2nd edn., CRC Press, Boca Raton, FL, (2007).
85. Lin, B. J., The k_3 coefficient in nonparaxial λ/NA scaling equations for resolution, depth of focus, and immersion lithography, *Journal of Microlithography Microfabrication and Microsystems*, **1**(1), 7 (2002).
86. Oldham, W. G. and Schenker, R. E., 193-nm lithographic system lifetimes as limited by UV compaction, *Solid State Technology*, **40**(4), 95–102 (1997).
87. Sewell, H., McClay, J., Jenkins, P. et al., 157 nm lithography—Window of opportunity, *Journal of Photopolymer Science and Technology*, **15**(4), 569 (2002).
88. Burnett, J. H., Levine, Z. H., and Shirley, E. L., Intrinsic birefringence in calcium fluoride and barium fluoride, *Physical Review B*, **64**(24), 241102 (2001).
89. Burnett, J. H., Levine, Z. H., Shirley, E. L., and Bruning, J. H., Symmetry of spatial-dispersion-induced birefringence and its implications for CaF_2 ultraviolet optics, *Journal of Microlithography Microfabrication and Microsystems*, **1**(3), 213 (2002).
90. Kang, H., Bourov, A., and Smith, B. W., Optical lithography at a 126-nm wavelength, *Emerging Lithographic Technologies V, SPIE*, **4343**, 797 (2001).
91. Liberman, V., Rothschild, M., Murphy, P. G., and Palmacci, S. T., Prospects for photolithography at 121 nm, *Journal of Vacuum Science & Technology B*, **20**(6), 2567 (2002).
92. Trintchouk, F., Ishihara, T., Gillespie, W. et al., XLA-300: The fourth-generation ArF MOPA light source for immersion lithography, *Optical Microlithography XIX, SPIE*, **6154**, 615423 (2006).
93. Wong, A. K. K., *Resolution Enhancement Techniques in Optical Lithography*, SPIE Press, Bellingham, WA, (2001).
94. Smayling, M. C., Liu, H. y., and Cai, L., Low k_1 logic design using gridded design rules, *Design for Manufacturability through Design-Process Integration II, SPIE*, **6925**, 69250B (2008).
95. Borodovsky, Y., Marching to the beat of Moore's Law, *Advances in Resist Technology and Processing XXIII, SPIE*, **6153**, 615301 (2006).
96. Bruning, J. H., Optical lithography: 40 years and holding, *Optical Microlithography XX, SPIE*, **6520**, 652004 (2007).
97. Matsuyama, T., Ohmura, Y., and Williamson, D. M., The lithographic lens: Its history and evolution, *Optical Microlithography XIX, SPIE*, **6154**, 615403 (2006).
98. Kawata, H., Carter, J., Yen, A., and Smith, H. I., Optical projection lithography using lenses with numerical apertures greater than unity, *Microelectronic Engineering*, **9**, 31 (1989).
99. Mulken, J., Flagello, D., Streefkerk, B., and Graeupner, P., Benefits and limitations of immersion lithography, *Journal of Microlithography Microfabrication and Microsystems*, **3**(1), 104 (2004).
100. Owen, G., Pease, R. F. W., Markle, D. A. et al., 1/8 μm optical lithography, *Journal of Vacuum Science & Technology B*, **10**(6), 3032 (1992).
101. de Klerk, J., Wagner, C., Droste, R. et al., Performance of a 1.35NA ArF immersion lithography system for 40-nm applications, *Optical Microlithography XX, SPIE*, **6520**, 65201Y (2007).
102. Lin, B., Drivers, prospects, and challenges for immersion lithography, *Third International Symposium on 157 nm Lithography*, Antwerp, Belgium (2002).
103. Owa, S., Shiraishi, N., Tanaka, I. et al., Nikon F2 exposure tool, *Third International Symposium on 157 nm Lithography*, Antwerp, Belgium (2002).
104. Smith, B. W., Kang, H., Bourov, A., and Cropanese, F., Extreme-NA water immersion lithography for 35–65 nm technology, *Third International Symposium on 157 nm Lithography*, Antwerp, Belgium (2002).
105. Switkes, M. and Rothschild, M., Resolution enhancement of 157-nm lithography by liquid immersion, *Optical Microlithography XV, SPIE*, **4691**, 459 (2002).
106. Adam, K. and Maurer, W., Polarization effects in immersion lithography, *Journal of Microlithography Microfabrication and Microsystems*, **4**(3), 031106 (2005).
107. Kunz, R. R., Switkes, M., Sinta, R. et al., Transparent fluids for 157-nm immersion lithography, *Journal of Microlithography Microfabrication and Microsystems*, **3**(1), 73 (2004).

AQ6

108. French, R. H., Qiu, W., Yang, M. K. et al., Second generation fluids for 193 nm immersion lithography, *Optical Microlithography XIX, SPIE*, **6154**, 615415 (2006).
109. Furukawa, T., Hieda, K., Wang, Y. et al., High refractive index fluid for next generation ArF immersion lithography, *Journal of Photopolymer Science and Technology*, **19**(5), 641 (2006).
110. Burnett, J. H., Kaplan, S. G., Shirley, E. L. et al., High-index optical materials for 193 nm immersion lithography, *Optical Microlithography XIX, SPIE*, **6154**, 615418 (2006).
111. Parthier, L., Wehrhan, G., Seifert, F. et al., Development update of high index lens material LuAG for ArF Hyper NA immersion systems, *Fifth International Symposium on Immersion Lithography Extensions*, The Hague, the Netherlands, 22–25 September 2008.
112. Jahromi, S., Bremer, L., Tuinier, R., and Liebrechts, S., Development of third generation immersion fluids based on dispersion of nanoparticles, *Fifth International Symposium on Immersion Lithography Extensions*, The Hague, the Netherlands, 22–25 September 2008.
113. Zimmerman, P., Rice, B., Rodriguez, R. et al., High index fluids to enable 1.55 and higher NA 193 nm immersion imaging, *Fifth International Symposium on Immersion Lithography Extensions*, The Hague, the Netherlands, 22–25 September 2008.
114. Zimmerman, P. A., Rice, B., Rodriguez, R. et al., The use of nanocomposite materials for high refractive index immersion lithography, *Journal of Photopolymer Science and Technology*, **21**(5), 621 (2008).
115. Byers, J., Lee, S., Jeri, K. et al., Double exposure materials: Simulation study of feasibility, *Journal of Photopolymer Science and Technology*, **20**(5), 707 (2007).
116. Hori, M., Nagai, T., Nakamura, A. et al., Sub-40-nm half-pitch double patterning with resist freezing process, *Advances in Resist Materials and Processing Technology XXV, SPIE*, **6923**, 69230H (2008).
117. Jung, W. Y., Kim, C. D., Eom, J. D. et al., Patterning with spacer for expanding the resolution limit of current lithography tool, *Design and Process Integration for Microelectronic Manufacturing IV, SPIE*, **6156**, 61561J (2006).
118. Reimer, L., *Transmission Electron Microscopy: Physics of Image Formation and Microanalysis*, 4th edn., Springer-Verlag, Berlin, Germany, (1985).
119. Bolorizadeh, M. and Joy, D. C., Effects of fast secondary electrons to low-voltage electron beam lithography, *Journal of Micro-Nanolithography MEMS and MOEMS*, **6**(2), 023004 (2007).
120. Baylor, L. R., Lowndes, D. H., Simpson, M. L. et al., Digital electrostatic electron-beam array lithography, *Journal of Vacuum Science & Technology B*, **20**(6), 2646 (2002).
121. Utsumi, T., Low-energy e-beam proximity lithography (LEEPL): Is the simplest the best? *Japanese Journal of Applied Physics Part 1-Regular Papers Short Notes & Review Papers*, **38**(12B), 7046 (1999).
122. Utsumi, T., Present status and future prospects of LEEPL, *Microelectronic Engineering*, **83**(4–9), 738 (2006).
123. Bethe, H., The theory of the passage of rapid neutron radiation through matter, *Annalen Der Physik*, **5**(3), 325 (1930).
124. Broers, A. N., Resolution limits of PMMA resist for exposure with 50 kV electrons, *Journal of the Electrochemical Society*, **128**(1), 166 (1981).
125. Tanuma, S., Powell, C. J., and Penn, D. R., Calculations of stopping powers of 100 eV to 30 keV electrons in 10 elemental solids, *Surface and Interface Analysis*, **37**(11), 978 (2005).
126. Han, G., Khan, M., Fang, Y. H., and Cerrina, F., Comprehensive model of electron energy deposition, *Journal of Vacuum Science & Technology B*, **20**(6), 2666 (2002).
127. Jackson, J. D., *Classical Electrodynamics*, 3rd edn., John Wiley & Sons Inc., New York, (1999).
128. Salisbury, I. G., Timsit, R. S., Berger, S. D., and Humphreys, C. J., Nanometer scale electron-beam lithography in inorganic materials, *Applied Physics Letters*, **45**(12), 1289 (1984).
129. Langheinrich, W. and Beneking, H., The resolution of the inorganic electron-beam resist LiF(AlF₃), *Microelectronic Engineering*, **23**(1–4), 287 (1994).
130. Muray, A., Isaacson, M., and Adesida, I., AlF₃—A new very high-resolution electron-beam resist, *Applied Physics Letters*, **45**(5), 589 (1984).
131. Yang, J. K. W. and Berggren, K. K., Using high-contrast salty development of hydrogen silsesquioxane for sub-10-nm half-pitch lithography, *Journal of Vacuum Science & Technology B*, **25**(6), 2025 (2007).
132. Parikh, M. and Kyser, D. F., Energy deposition functions in electron resist films on substrates, *Journal of Applied Physics*, **50**(2), 1104 (1979).
133. Watson, G. P., Berger, S. D., Liddle, J. A. et al., Precise measurement of the effective backscatter coefficient for 100-keV electron-beam lithography on Si, *Journal of Vacuum Science & Technology B*, **13**(6), 2535 (1995).
134. Watson, G. P., Fetter, L. A., and Liddle, J. A., Dose modification proximity effect correction scheme with inherent forward scattering corrections, *Journal of Vacuum Science & Technology B*, **15**(6), 2309 (1997).
135. Owen, G. and Rissman, P., Proximity effect correction for electron-beam lithography by equalization of background dose, *Journal of Applied Physics*, **54**(6), 3573 (1983).
136. Watson, G. P., Berger, S. D., Liddle, J. A., and Waskiewicz, W. K., A background dose proximity effect correction technique for scattering with angular limitation projection electron lithography implemented in hardware, *Journal of Vacuum Science & Technology B*, **13**(6), 2504 (1995).
137. Groves, T. R., Efficiency of electron-beam proximity effect correction, *Journal of Vacuum Science & Technology B*, **11**(6), 2746 (1993).
138. Seo, E. and Kim, O., Dose and shape modification proximity effect correction for forward-scattering range scale features in electron beam lithography, *Japanese Journal of Applied Physics Part 1-Regular Papers Short Notes & Review Papers*, **39**(12B), 6827 (2000).

139. Lee, S. Y., Jacob, J. C., Chen, C. M., Mcmillan, J. A., and Macdonald, N. C., Proximity effect correction in electron-beam lithography—A hierarchical rule-based scheme-pyramid, *Journal of Vacuum Science & Technology B*, **9**(6), 3048 (1991).
140. Patrick, W. and Vettiger, P., Optimization of the proximity parameters for the electron-beam exposure of nanometer gate-length GaAs metal-semiconductor field-effect transistors, *Journal of Vacuum Science & Technology B*, **6**(6), 2037 (1988).
141. Wuest, R., Strasser, P., Jungo, M. et al., An efficient proximity-effect correction method for electron-beam patterning of photonic-crystal devices, *Microelectronic Engineering*, **67-8**, 182 (2003).
142. Jansen, G. H., *Coulomb Interactions in Particle Beams*, Academic Press, New York, (1990).
143. Mkrtchyan, M. M., Liddle, J. A., Berger, S. D. et al., Stochastic scattering in charged particle projection systems: A nearest neighbor approach, *Journal of Applied Physics*, **78**(12), 6888 (1995).
144. Stickel, W., Simulation of Coulomb interactions in electron beam lithography systems—A comparison of theoretical models, *Journal of Vacuum Science & Technology B*, **16**(6), 3211 (1998).
145. Gallatin, G. M. and Liddle, J. A., Analytical model of the “Shot Noise” effect in photoresist, *Microelectronic Engineering*, **46**(1-4), 365 (1999).
146. Gallatin, G. M., Continuum model of shot noise and line edge roughness, *Lithography for Semiconductor Manufacturing II, SPIE*, **4404**, 123 (2001).
147. Kruit, P., Steenbrink, S., and Wieland, M., Predicted effect of shot noise on contact hole dimension in e-beam lithography, *Journal of Vacuum Science & Technology B*, **24**(6), 2931 (2006).
148. Neureuther, A. R., Pease, R. F. W., Yuan, L. et al., Shot noise models for sequential processes and the role of lateral mixing, *Journal of Vacuum Science & Technology B*, **24**(4), 1902 (2006).
149. Smith, H. I., A statistical-analysis of ultraviolet, x-ray, and charged-particle lithographies, *Journal of Vacuum Science & Technology B*, **4**(1), 148 (1986).
150. Ferrera, J., Wong, V. V., Rishton, S. et al., Spatial-phase-locked electron-beam lithography—Initial test-results, *Journal of Vacuum Science & Technology B*, **11**(6), 2342 (1993).
151. Fares, N., Stanton, S., Liddle, J., and Gallatin, G., Analytical-based solutions for SCALPEL wafer heating, *Journal of Vacuum Science & Technology B*, **18**(6), 3115 (2000).
152. Babin, S. and Kuzmin, I. Y., Experimental verification of the TEMPTATION (temperature simulation) software tool, *Journal of Vacuum Science & Technology B*, **16**(6), 3241 (1998).
153. Chao, W. L., Harteneck, B. D., Liddle, J. A., Anderson, E. H., and Attwood, D. T., Soft x-ray microscopy at a spatial resolution better than 15 nm, *Nature*, **435**(7046), 1210 (2005).
154. Sturans, M. A., Hartley, J. G., Pfeiffer, H. C. et al., EL5: One tool for advanced x-ray and chrome on glass mask making, *Journal of Vacuum Science & Technology B*, **16**(6), 3164 (1998).
155. Nakayama, Y., Okazaki, S., Saitou, N., and Wakabayashi, H., Electron-beam cell projection lithography—A new high-throughput electron-beam direct-writing technology using a specially tailored Si aperture, *Journal of Vacuum Science & Technology B*, **8**(6), 1836 (1990).
156. Pfeiffer, H. C., Projection reduction exposure with variable axis immersion lenses (PREVAIL)—A high throughput e-beam projection approach for next generation lithography, *Japanese Journal of Applied Physics Part 1-Regular Papers Short Notes & Review Papers*, **38**(12B), 7022 (1999).
157. Heritage, M. B., Electron-projection microfabrication system, *Journal of Vacuum Science & Technology*, **12**(6), 1135 (1975).
158. <http://www.darpa.mil/MTO/Programs/nanowriter/index.html>, 2009.
159. Kruit, P., High throughput electron lithography with the multiple aperture pixel by pixel enhancement of resolution concept, *Journal of Vacuum Science & Technology B*, **16**(6), 3177 (1998).
160. Chang, T. H. P., Thomson, M. G. R., Kratschmer, E. et al., Electron-beam microcolumns for lithography and related applications, *Journal of Vacuum Science & Technology B*, **14**(6), 3774 (1996).
161. Groves, T. R. and Kendall, R. A., Distributed, multiple variable shaped electron beam column for high throughput maskless lithography, *Journal of Vacuum Science & Technology B*, **16**(6), 3168 (1998).
162. Pease, R. F. and Chou, S. Y., Lithography and other patterning techniques for future electronics, *Proceedings of IEEE*, **96**(2), 248 (2008).
163. Sreenivasan, S. V., Nanoscale manufacturing enabled by imprint lithography, *MRS Bulletin*, **33**(9), 854 (2008).
164. Barty, A. and Goldberg, K. A., The effects of radiation induced carbon contamination on the performance of an EUV lithographic optic, *Proceedings of SPIE*, **5037**, 450 (2003).
165. Brainard, R. L., Henderson, C., Cobb, J. et al., Comparison of the lithographic properties of positive resists upon exposure to deep- and extreme-ultraviolet radiation, *Journal of Vacuum Science & Technology B*, **17**, 3384 (1999).
166. Brainard, R. L., Barclay, G. G., Anderson, E. H., and Ocola, L. E., Resists for next generation lithography, *Microelectronic Engineering*, **62**(707), 715 (2002).
167. Chou, S. Y., Krauss, P. R., and Renstrom, P. J., Imprint of sub-25 nm vias and trenches in polymers, *Applied Physics Letters*, **67**(21), 3114 (1995).
168. Chou, S. Y., Krauss, P. R., and Renstrom, P. J., Imprint lithography with 25-nanometer resolution, *Science*, **272**(5258), 85 (1996).

169. Haisma, J., Verheijen, M., vandenHeuvel, K., and van den Berg, J., Mold-assisted nanolithography: A process for reliable pattern replication, *Journal of Vacuum Science & Technology B*, **14**(6), 4124 (1996).
170. Colburn, M., Johnson, S., Stewart, M. et al., Step and flash imprint lithography: A new approach to high-resolution patterning, *Proceedings of SPIE*, **3676**, 379 (1999).
171. Bratton, D., Yang, D., Dai, J. Y., and Ober, C. K., Recent progress in high resolution lithography, *Polymers for Advanced Technologies*, **17**(2), 94 (2006).
172. Gao, H., Tan, H., Zhang, W., Morton, K., and Chou, S. Y., Air cushion press for excellent uniformity, high yield, and fast nanoimprint across a 100 mm field, *Nano Letters*, **6**(11), 2438 (2006).
173. Huang, X. D., Bao, L. R., Cheng, X. et al., Reversal imprinting by transferring polymer from mold to substrate, *Journal of Vacuum Science & Technology B*, **20**(6), 2872 (2002).
174. Schmid, G. M., Stewart, M. D., Wetzel, J. et al., Implementation of an imprint damascene process for interconnect fabrication, *Journal of Vacuum Science & Technology B*, **24**(3), 1283 (2006).
175. Kim, K., Jeong, J., Park, S. et al., Development of a very large-area ultraviolet imprint lithography process, *Microelectronic Engineering*, in press 86,1983-1988(2009).
176. Ahn, S. H. and Guo, L. J., High-speed roll-to-roll nanoimprint lithography on flexible plastic substrates, *Advanced Materials*, **20**(11), 2044 (2008).
177. Tan, H., Gilbertson, A., and Chou, S. Y., Roller nanoimprint lithography, *Journal of Vacuum Science & Technology B*, **16**(6), 3926 (1998).
178. Ahn, S. H., Kim, J. S., and Guo, L. J., Bilayer metal wire-grid polarizer fabricated by roll-to-roll nanoimprint lithography on flexible plastic substrate, *Journal of Vacuum Science & Technology B*, **25**(6), 2388 (2007).
179. PolyIC. <http://www.polyic.com>, 2009.
180. Hua, F., Sun, Y. G., Gaur, A. et al., Polymer imprint lithography with molecular-scale resolution, *Nano Letters*, **4**(12), 2467 (2004).
181. Austin, M. D., Zhang, W., Ge, H. X. et al., 6 nm half-pitch lines and 0.04 μm^2 static random access memory patterns by nanoimprint lithography, *Nanotechnology*, **16**(8), 1058 (2005).
182. Ding, Y. F., Ro, H. W., Germer, T. A. et al., Relaxation behavior of polymer structures fabricated by nanoimprint lithography, *ACS Nano*, **1**(2), 84 (2007).
183. Ding, Y. F., Ro, H. W., Alvine, K. J. et al., Nanoimprint lithography and the role of viscoelasticity in the generation of residual stress in model polystyrene patterns, *Advanced Functional Materials*, **18**(12), 1854 (2008).
184. Jones, R. L., Hu, T. J., Soles, C. L. et al., Real-time shape evolution of nanoimprinted polymer structures during thermal annealing, *Nano Letters*, **6**(8), 1723 (2006).
185. Hirai, Y., Yoshida, S., and Takagi, N., Defect analysis in thermal nanoimprint lithography, *Journal of Vacuum Science & Technology B*, **21**(6), 2765 (2003).
186. Jung, G. Y., Li, Z. Y., Wu, W. et al., Vapor-phase self-assembled monolayer for improved mold release in nanoimprint lithography, *Langmuir*, **21**(4), 1158 (2005).
187. Miller, M., Brooks, C., Lentz, D. et al., Step and flash imprint process integration techniques for photonic crystal patterning: Template replication through wafer patterning irrespective of tone, *Proceedings of SPIE*, **6883**, 68830D (2008).
188. *International Technology Roadmap for Semiconductors*, 2007 edition, <http://www.itrs.net>, Metrology. SEMATECH, Austin, TX
189. Li, M. T., Chen, L., Zhang, W., and Chou, S. Y., Pattern transfer fidelity of nanoimprint lithography on six-inch wafers, *Nanotechnology*, **14**(1), 33 (2003).
190. Lee, H. J., Ro, H. W., Soles, C. L. et al., Effect of initial resist thickness on residual layer thickness of nanoimprinted structures, *Journal of Vacuum Science & Technology B*, **23**, 3023 (2005).
191. Schulz, H., Wissen, M., and Scheer, H. C., Local mass transport and its effect on global pattern replication during hot embossing, *Microelectronic Engineering*, **67-68**, 657 (2003).
192. Kim, K. D., Jeong, J. H., Sim, Y. S., and Lee, E. S., Minimization of residual layer thickness by using the optimized dispensing method in S-FIL (TM) process, *Microelectronic Engineering*, **83**, 847 (2006).
193. Melliar-Smith, M., Lithography beyond 32 nm—A role for imprint? *Proceedings of SPIE*, **6520**, 652001 (2007).
194. Zhang, W. and Chou, S. Y., Multilevel nanoimprint lithography with submicron alignment over 4 in. Si wafers, *Applied Physics Letters*, **79**(6), 845 (2001).
195. Resnick, D. J., Dauksher, W. J., Mancini, D. et al., Imprint lithography for integrated circuit fabrication, *Journal of Vacuum Science & Technology B*, **21**(6), 2624 (2003).
196. Jung, G. Y., Johnston-Halperin, E., Wu, W. et al., Circuit fabrication at 17 nm half-pitch by nanoimprint lithography, *Nano Letters*, **6**(3), 351 (2006).
197. Hand, A., *Toshiba Validates Imprint Lithography for < 32 nm*, Semiconductor International, October, (2007).
198. Hart, M. W. IBM Almaden RC, DARPA Presentation. 2007.
199. Dobisz, E. A., Bandic, Z. Z., Tsai-Wei, W., and Albrecht, T., Patterned media: Nanofabrication challenges of future disk drives, *Proceedings of IEEE*, **96**(11), 1836 (2008).
200. Ahn, S. W., Lee, K. D., Kim, J. S. et al., Fabrication of a 50 nm half-pitch wire grid polarizer using nanoimprint lithography, *Nanotechnology*, **16**(9), 1874 (2005).
201. Yu, Z. N., Deshpande, P., Wu, W., Wang, J., and Chou, S. Y., Reflective polarizer based on a stacked double-layer sub-wavelength metal grating structure fabricated using nanoimprint lithography, *Applied Physics Letters*, **77**(7), 927 (2000).
202. Raymond, C., Scatterometry for semiconductor metrology, in A. C. Diebold (ed.), *Handbook of Silicon Semiconductor Metrology*, Dekker, New York, p. 477 (2001).
203. SEMI Standard. Test method for evaluation of line edge roughness and line width roughness, SEMI P47-0307.

204. Jones, R. L., Lin, E. K., Lin, Q. et al., Cross-section and critical dimension metrology in dense high aspect ratio patterns with CD-SAXS, *AIP Conference Proceedings*, **788**, 403 (2005).
205. Notte, J., Ward, B., Economou, N. et al., An introduction to the helium ion microscope, *AIP Conference Proceedings*, **931**, 489 (2007).
206. Wang, C. Q., Jones, R. L., Lin, E. K. et al., Characterization of correlated line edge roughness of nanoscale line gratings using small angle x-ray scattering, *Journal of Applied Physics*, **102**(2), 024901 (2007).
207. Wang, C. Q., Jones, R. L., Lin, E. K., Wu, W. L., and Leu, J., Small angle x-ray scattering measurements of lithographic patterns with sidewall roughness from vertical standing waves, *Applied Physics Letters*, **90**(19), 193122-3 (2007).
208. Hu, T. J., Jones, R. L., Wu, W. L. et al., Small angle x-ray scattering metrology for sidewall angle and cross section of nanometer scale line gratings, *Journal of Applied Physics*, **96**(4), 1983 (2004).
209. Jones, R. L., Hu, T., Lin, E. K. et al., Small angle x-ray scattering for sub-100 nm pattern characterization, *Applied Physics Letters*, **83**(19), 4059 (2003).

Author Queries

[AQ1] Please check if these two paragraphs, “Official ... for this purpose.” be either deleted or moved as a note.

[AQ2] Please review the sentence beginning with “Finally, in Section 19.6 ...” for clarity

[AQ3] In the sentence beginning with “The line-width variations...” is half-pitch the correct definition for HP?

[AQ4] References [12, 14, 31, 121] are exactly the same as references [40, 33, 38, 128]. Hence repeated references are deleted and renumbered in the list as well as in the text. Please check.

[AQ5] Please update Refs. [67,175,198].

[AQ6] Please provide the year of publication for Refs. [102–104].

